# Efficient Molecular Mechanics for Chemical Reactions: Multiconfiguration Molecular Mechanics Using Partial Electronic Structure Hessians

**Hai Lin,[†] Jingzhi Pu,[†] Titus V. Albu,[‡] and Donald G. Truhlar*,[†]**

*Department of Chemistry and Supercomputer Institute, University of Minnesota, Minneapolis, Minnesota 55455-0431 and Department of Chemistry, Tennessee Technological University, Box 5055, Cookeville, Tennessee 38505*

*Received: January 2, 2004; In Final Form: February 24, 2004*

Multiconfiguration molecular mechanics (MCMM) is a method for representing polyatomic potential energy surfaces by combining molecular mechanics potentials for the reactant and product wells with electronic structure data (energy, gradient, and Hessian) at the saddle point and a small number of nonstationary points. A general strategy for placement of the nonstationary points has been developed [Albu, T. V.; Corchado, J. C.; Truhlar, D. G. *J. Phys. Chem. A* **2001**, *105*, 8465] for fitting potential energy surfaces in the vicinity of the reaction path and in the reaction swath region and for calculating rate constants for atom transfer reactions by variational transition state theory with multidimensional tunneling. In the present work, we improve the efficiency of the MCMM method by using electronic structure calculations only for certain critical elements of the Hessians at the nonstationary points and by using interpolation for the other elements at the nonstationary points. We tested this new MCMM strategy for a diverse test suite of six reactions involving hydrogen-atom transfer. The new method yields quite accurate rate constants as compared with the standard MCMM strategy employing full electronic structure Hessians and also as compared with direct dynamics calculations using an uninterpolated full potential energy surface at the same electronic structure level. In comparison with the standard MCMM strategy, this new procedure reduces the computational effort associated with the nonstationary points by a factor of up to 3 for the test reactions and up to 11 for even larger reactive systems.

## 1. Introduction

Variational transition state theory with multidimensional tunneling contributions (VTST/MT) has been established as a powerful method for studying chemical reaction dynamics.[1−8] A successful application usually relies on the accuracy of the potential energy surface (PES), especially in the reaction swath. The reaction swath is defined as the union of the narrow valley centered along the minimum energy path (MEP) that connects the reactants and products and the wider region on the concave side of the MEP that is associated with large-curvature tunneling (LCT, i.e., extensive nonclassical corner cutting).[6,9] Generation of the PES in the reaction swath requires correlated electronic structure theory[10−20] since molecular mechanics potential functions,[21−26] which are useful for modeling reactants and products, are incapable of describing bond breaking and bond forming. One way to proceed is direct dynamics,[9,27−49] where the electronic structure PES is calculated on the fly. However, applications of direct dynamics are still limited to relatively small reactive systems due to the high computational costs of electronic structure calculations. Therefore, it is desirable to develop algorithms that allow the generation of reactive PESs with minimal computational effort.

Recently, we introduced an efficient algorithm for this purpose; the algorithm is called multiconfiguration molecular mechanics (MCMM).[50,51] This is a dual-level scheme that uses molecular mechanics potential functions as the nominally lower-level data and electronic structure theory for the higher-level data. This is accomplished by forming an electronically nonadiabatic (i.e., diabatic) Hamiltonian matrix **V** whose diagonal elements are given by classical molecular mechanics and whose off-diagonal elements are obtained by Shepard interpolation of quadratic expansions around a set of points where the higher-level electronic structure data is available. The nonadiabatic representation is not unique, and the choice made for MCMM is a valence bond Hamiltonian, in which $V_{11}$ ($V_{22}$) is the energy of a valence bond state with the reactant's (product's) bonding pattern, and $V_{12}$ is the resonance energy. This kind of nondiagonal representation of the Hamiltonian has been used in a variety of contexts for modeling reactive systems.[29,52−96] In MCMM, the Born−Oppenheimer potential energy surface is obtained as the lowest eigenvalue of the matrix **V**, and it reproduces the higher-level data in the vicinity of each electronic structure data point. The MCMM method is therefore a general fitting scheme for creating semiglobal PESs for reactive systems.

The MCMM method allows one to carry out the entire dynamics calculation from a reasonably small amount of electronic structure data without requiring the human judgment traditionally associated with the "art" of fitting multidimensional functions. The whole MCMM fitting process is unique and automatic except for the decision about where to locate the input data. In principle the results converge to a numerically accurate interpolation of the PES for any reasonable scheme of adding data. In our second paper on this subject,[51] we developed a practical scheme for locating the data that minimizes the number of points at which data is used. In addition to the reactant- and product-valley wells (which are the reactants' complex and products' complex for bimolecular reactions with two products), which are described by molecular mechanics functions, we employed up to 11 points where electronic structure data were

[†] University of Minnesota.
[‡] Tennessee Technological University.

10.1021/jp049972+ CCC: $27.50 
Published on Web 04/07/2004

determined. These points include the saddle point and 10 supplementary nonstationary points. (The nonstationary points are not necessarily on the MEP, although seven of these are close to the MEP of the final MCMM surface.) This scheme was validated by tests against a diverse set of reactions involving hydrogen transfer; such reactions tend to be very challenging with respect to determining both variational and tunneling effects. The validation suite included both cases dominated by small-curvature tunneling (SCT)[35,97] and cases dominated by large-curvature tunneling (LCT)[5,6,8,9,36,37,97−103] Accurate rate constants were obtained, even for LCT-dominated reactions, which require PES information over a more extensive region than is required for SCT calculations.

Electronic structure data that are used in a standard MCMM calculation include energies, gradients, and Hessians. The Hessians are the most expensive items to compute, especially when they are not analytically available but have to be calculated numerically. The cost associated with the evaluation of high-level Hessians prevents the straightforward application of MCMM to converge the PES for very large reactive systems. The objective of the present paper is to improve the "standard" MCMM method by reducing the effort required for Hessian computations. This is accomplished by use of partial electronic structure Hessians, i.e., use of electronic structure for certain critical Hessian elements with approximate values for the other Hessian elements. Details will be presented in section 2. This new strategy will be tested against straight direct dynamics calculations for the following reactions:

$$O + CH_4 \rightarrow OH + CH_3 \quad \text{(R-1)}$$

$$OH + CH_4 \rightarrow H_2O + CH_3 \quad \text{(R-2)}$$

$$NH_2 + CH_4 \rightarrow NH_3 + CH_3 \quad \text{(R-3)}$$

$$CH_2F + CH_3Cl \rightarrow CH_3F + CH_2Cl \quad \text{(R-4)}$$

$$OH + C_3H_8 \rightarrow H_2O + CH_3CHCH_3 \quad \text{(R-5)}$$

$$OH + C_3H_8 \rightarrow H_2O + CH_2CH_2CH_3 \quad \text{(R-6)}$$

Five of these reactions (R-1 through R-5) have been already included in the previous tests[51] for the standard scheme. The newly introduced R-6 has the same reactants as R-5 but the reaction takes place at the primary instead of secondary C position of propane. Computational details and results will be given in section 3, where comparisons between MCMM with the new partial-Hessian scheme, MCMM with the standard[51] scheme, and direct dynamics calculations will be tabulated. Section 4 contains a discussion.

## 2. Multiconfiguration Molecular Mechanics

**2.1. Overview.** In this section, we briefly review the standard MCMM algorithm.[50] Details of the algorithm can be obtained from the original paper[50] and will not be repeated here.

The Born−Oppenheimer potential energy is represented at a geometry defined in internal coordinates $\mathbf{q}$ as the lowest eigenvalue of a $2 \times 2$ electronically diabatic Hamiltonian matrix $\mathbf{V}(\mathbf{q})$:

$$\mathbf{V}(\mathbf{q}) = \begin{pmatrix} V_{11}(\mathbf{q}) & V_{12}(\mathbf{q}) \\ V_{12}(\mathbf{q}) & V_{22}(\mathbf{q}) \end{pmatrix} \quad (1)$$

where the $V_{11}$ and $V_{22}$ elements are classical molecular mechanics potential functions that describe reactant well and product well valence bond configurations, respectively, and the $V_{12}$ element is the resonance integral. The lowest eigenvalue is

$$V(\mathbf{q}) = \frac{1}{2}\{(V_{11}(\mathbf{q}) + V_{22}(\mathbf{q})) - [(V_{11}(\mathbf{q}) - V_{22}(\mathbf{q}))^2 + 4V_{12}(\mathbf{q})^2]^{1/2}\} \quad (2)$$

The first and second derivatives of $V(\mathbf{q})$, which are required for the dynamical calculations, are obtained by differentiation of eq 2, after we know $V_{11}(\mathbf{q})$, $V_{22}(\mathbf{q})$, and $V_{12}(\mathbf{q})$. The molecular mechanics potentials $V_{11}(\mathbf{q})$ and $V_{22}(\mathbf{q})$ are readily available, inexpensive to calculate, and "easy" to differentiate analytically. The resonance integral $V_{12}(\mathbf{q})$ and its derivatives are the key features of the MCMM algorithm, and they are obtained using Shepard interpolation.[104,105]

The interpolation is based on data at a set of $M$ points called Shepard points $\mathbf{q}^{(k)}$, with $k = 1, 2, ..., M$, at which the energies $V^{(k)}$, gradients $\mathbf{g}^{(k)}$, and Hessian matrices $\mathbf{f}^{(k)}$ are available. For a given Shepard point $\mathbf{q}^{(k)}$, $V(\mathbf{q};k)$ is expanded in a Taylor series around $\mathbf{q}^{(k)}$. After expanding $V_{11}(\mathbf{q};k)$ and $V_{22}(\mathbf{q};k)$ using molecular mechanics potential functions, a quadratic expansion of $V_{12}(\mathbf{q};k)$ around point $\mathbf{q}^{(k)}$ is obtained following ref 74 and using eq 2; this was given as eq 13 in ref 50. This quadratic expansion is carried out in internal coordinates[50] to avoid any ambiguity of the orientation of the system in space.

Once the quadratic expansion of $V_{12}(\mathbf{q};k)$ is completed for all the Shepard points, $V_{12}$ at a desired geometry $\mathbf{q}$ (in internal coordinates) can be evaluated by means of Shepard interpolation as a linear combination of the quadratic expansions around these Shepard points:

$$V_{12}^{S}(\mathbf{q}) = \sum_{k=1}^{M} W_k(\mathbf{q}) V_{12}^{\mathrm{mod}}(\mathbf{q};k) \quad (3)$$

where the S superscript in $V_{12}^{S}(\mathbf{q})$ indicates that $V_{12}$ is obtained via Shepard interpolation, $W_k(\mathbf{q})$ are normalized weights, and $V_{12}^{\mathrm{mod}}(\mathbf{q};k)$ is a modified quadratic function:

$$[V_{12}^{\mathrm{mod}}(\mathbf{q};k)]^2 = [V_{12}(\mathbf{q};\mathrm{k})]^2\, u(\mathbf{q};k) \quad (4)$$

where the modification is[50]

$$u(\mathbf{q};k) = \begin{cases} \exp\{-\delta/[V_{12}(\mathbf{q};k)]^2\} & [V_{12}(\mathbf{q};k)]^2 > 0 \\ 0 & [V_{12}(\mathbf{q};k)]^2 \le 0 \end{cases} \quad (5)$$

with $\delta = 1 \times 10^{-8} E_h^2$ (note: $1E_h = 1$ hartree $= 627.51$ kcal/mol). The weight functions, $W_k(\mathbf{q})$, are one of the keys to the success of the method; they are the smoothest functions that satisfy the required energy and derivative conditions at the Shepard points, as discussed in ref 50. In particular, the functional form that we adopted is[50]

$$W_k(\mathbf{q}) = \left(\frac{1}{d_k(\mathbf{q})}\right)^4 \Big/ \sum_{i=1}^{M}\left(\frac{1}{d_i(\mathbf{q})}\right)^4 \quad (6)$$

where $d_k(\mathbf{q})$ denotes a generalized distance between $\mathbf{q}$ and $\mathbf{q}^{(k)}$ defined as

$$d_k(\mathbf{q}) = \sqrt{\sum_{j=1}^{j_{\max}} (q_j - q_j^{(k)})^2} \quad (7)$$

The first and second derivatives of $V_{12}^S(\mathbf{q})$ are evaluated using eqs 26 and 27 of ref 50, respectively. $V(\mathbf{q})$ and its first and second derivatives can be computed accordingly (eqs 5 to 7 in ref 50).

In our studies, the internal coordinates used to calculate the generalized distance in eq 7 are three ($j_{max} = 3$) interatomic distances ($q_1$, $q_2$ and $q_3$) that change significantly during reaction—(i) the forming bond distance, (ii) the breaking bond distance, and (iii) the distance between the nontransferring atoms involved in these bonds.

A Shepard interpolation in the MCMM algorithm requires at least three points, which are the minima of the reactant- and product-valley wells and the saddle point. These first three points are all stationary points, and they are the first three Shepard points ($k = 1$, 2, and 3) employed in all cases. An MCMM calculation based on these three points without any supplementary points is denoted as MCMM-0. Then $N_s$ supplementary points can be added successively into the Shepard interpolation, and the corresponding MCMM computation (based overall on $M = N_s + 3$ points) is labeled MCMM-$N_s$. In the standard MCMM interpolation scheme as well as the improved scheme used in this paper, the reactant- and product-valley wells are completely described at the molecular mechanics level, whereas the other Shepard points (the saddle point and supplementary points) are treated at the higher-level of theory, i.e., using electronic structure calculations. Therefore, to generate the MCMM potential energy surface, one needs higher-level electronic structure data (energy, gradient, and Hessian) at $N_s + 1$ points.

To perform variational transition state theory computations, additional electronic structure information is required for the reactants, and to calculate the equilibrium constant or reverse rates, such information is required for products. For MCMM, one needs the product energy even if one only wants forward rates because the reactant and product relative energies are needed to determine the energy difference between $V_{22}$ and $V_{11}$, since the zero of energy for a given valence bonding pattern in a molecular mechanics computation is arbitrary. We also require the Hessians for the reactants in order to compute their vibrational partition function, and we require Hessians for both reactants and products to carry out the tunneling calculations.

**2.2. Location of Supplementary Shepard Points.** As pointed out before,[51] in principle the computed reaction rates converge to the results obtained on a numerically accurate interpolation of the PES (or, equivalently, the results obtained by direct dynamics) for any reasonable scheme of adding data. From a practical point of view, it is convenient to have a standard strategy for adding points. This problem was explored in our previous study and a general scheme of successively adding supplementary Shepard points was proposed.[51] (For the convenience of the readers, Table S-1 of the Supporting Information reviews the sequence for adding supplementary points in the standard scheme.) In this process, the location of the $\alpha$th ($\alpha = 1, 2, ..., N_s$) supplementary point is based on the information along the MEP given in the MCMM-($\alpha - 1$) calculation. Such information includes both the potential energy surface along the minimum energy path, $V_{MEP}(s)$, and the vibrationally adiabatic ground-state potential energy curve,[1,4] $V_a^G(s)$, where $s$ denotes the signed distance from the saddle point along the mass-scaled reaction coordinate,[1,4] and $V_a^G(s)$ is obtained by adding the zero point energy of the modes transverse to the reaction path to $V_{MEP}(s)$. The maximum of the $V_a^G(s)$ curve, which corresponds to the dynamical bottleneck at 0 K,[106] and its location along the MEP are denoted $V_a^{AG}$ and $s_*^{AG}$ respectively. One also takes into account the values from electronic structure calculations (these do not depend on the MCMM algorithm) at the reactants, the products, and the saddle point—$V^R$, $V^P$, and $V^{\ddagger}$ for $V_{MEP}(s)$, and $V_a^{RG}$, $V_a^{PG}$, and $V_a^{\ddagger G}$ for $V_a^G(s)$, respectively. (See Figure 1 in ref 51) The forward and backward barrier heights are labeled $V^{\ddagger}$ and $V_{rev}^{\ddagger}$, respectively, and $\bar{V}^{\ddagger}$ is their average; $V^R$ is always taken as the zero of energy for a given reaction.

The algorithm for adding the supplementary Shepard points does not depend on the direction of a reaction, i.e., from the reactants to products or from products to reactants. Instead, it depends on the locations of the high- and low-energy sides of a reaction profile, which will be called simply the high and low sides. The high side is the reactant side and the low side is the product side if $V_a^{RG} > V_a^{PG}$, and vice versa. $V^H$ and $V^L$ indicates the $V_{MEP}(s)$ value at the high and low side, respectively (i.e., at $s = -\infty$ and $+\infty$ if $V_a^{RG} > V_a^{PG}$ or at $s = +\infty$ and $-\infty$ if $V_a^{RG} < V_a^{PG}$). Similarly, $V_a^{HG}$ and $V_a^{LG}$ denote the corresponding $V_a^G(s)$ values on the high and low sides, respectively. Furthermore, an intrinsic barrier height ($V_{int}^{\ddagger}$) is defined as the potential energy difference between the saddle point ($s = 0$) and the high side, i.e.,

$$V_{int}^{\ddagger} \equiv V_{MEP}(s = 0) - V^H \tag{8}$$

The dynamical bottleneck side is the side on which $s_*^{AG}$ occurs.

The first seven supplementary points are on the MEP. The eighth through the tenth supplementary points are on the concave side of the MEP region and are determined on the basis of the locations of the assistant points $8_H/8_L$, $9_H/9_L$, and $10_H/10_L$, respectively. These assistant points are on the MEP, and the subscripts H/L indicate their locations on the high/low sides.

**2.3. Less Expensive Treatment of Hessians.** In generating the PES, the standard MCMM scheme requires electronic structure data (energy, gradient, and Hessian) at the saddle point and supplementary points. The optimization of the saddle point, the computation of its normal modes, and the evaluation of Hessians at the $N_s$ nonstationary points by electronic structure calculations are the most computationally costly steps. We introduce here a less expensive way to treat the Hessians of the nonstationary points.

The basic idea comes from the observation that normally only a portion of the atoms in a reaction are directly involved in bond breaking and forming or in change of bond order. These atoms are called core atoms. It is expected that the Hessian elements that involve only the core atoms might be more critical than the other Hessian elements. Our improvement to the standard method is to treat these critical elements accurately by electronic structure calculations and to approximate the other elements in an appropriate manner.

In our scheme, we group the atoms into four layers: (1) core atoms, which are normally the ones that are directly involved in bond breaking and forming or that change their bond orders, (2) geminal atoms that are bonded to the core atoms, (3) vicinal atoms that are bonded to the geminal atoms, (4) and the remaining atoms, which are called "distant" atoms. This is illustrated in Figure 1 for reaction R-6, for which one has three core, four geminal, three vicinal, and three distant atoms.

Generally, the core atoms should be selected on the basis of the importance of the role that an atom plays in the reaction. For example, in electrocyclic reactions,[107] some bonds do not break but their bond orders change. In such a case, the core atoms should include all atoms whose bond order to any other atom changes. (Thus, one has the option to include more atoms

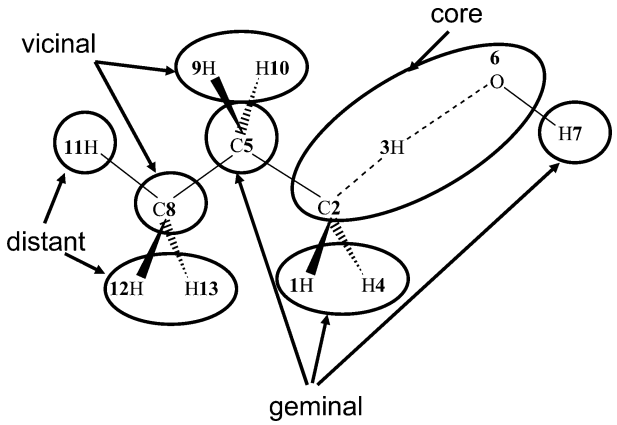


**Figure 1.** Atom groups for the reaction OH + $C_3H_8$ → $H_2O$ + $CH_2$-$CH_2CH_3$.

| | Core | Gem | Vic | Dist |
|---|---|---|---|---|
| Core | 0–10 | 0–5 | 0–3 | 0 |
| Gem | 0–5 | 0–5 | 0–3 | 0 |
| Vic | 0–3 | 0–3 | 0–3 | 0 |
| Dist | 0 | 0 | 0 | 0 |

**Figure 2.** Use of electronic structure Hessian components for the saddle point (Shepard point 0) and supplementary points (Shepard points 1−10) in MCMM-10/3v2g5c. Gem for geminal, Vic for vicinal, and Dist for distant.

| | Core | Gem | Vic | Dist |
|---|---|---|---|---|
| Core | 0–10 | 0–4 | 0–2 | 0 |
| Gem | 0–4 | 0–4 | 0–2 | 0 |
| Vic | 0–2 | 0–2 | 0–2 | 0 |
| Dist | 0 | 0 | 0 | 0 |

**Figure 3.** Use of electronic structure Hessian components for the saddle point (Shepard point 0) and supplementary points (Shepard points 1−10) in MCMM-10/2v2g6c. Gem for geminal, Vic for vicinal, and Dist for distant.

in the core, but in the applications presented here there will always be three core atoms.)

In our new strategy to treat the Hessian elements, the number of atoms for which Hessian elements are evaluated by electronic structure calculations is reduced gradually as more and more supplementary Shepard points are added. Various options may be considered depending on how this is done. At the beginning, the list of atoms for which Hessian elements are computed by electronic structure calculations could include all the atoms or it could include core, geminal, and vicinal atoms. We abbreviate such an atom list as "v" since the outermost layer is made of the vicinal atoms. Similarly, "g" labels an atom list with core and geminal atoms, and "c" indicates an atom list with only core atoms. If all atoms are included, however, we prefer "a" (which stands for "all") to "d" (stands for "distant"). The key idea is that all elements of the Hessian at the saddle point are obtained from an electronic structure calculation, but as one moves to supplementary points, the atom list for electronic structure Hessian elements switches to "v", then "g", and finally ends up at "c".

Figures 2 and 3 illustrate respectively two options, 10/3v2g5c and 10/2v2g6c, which are investigated in this work. The 10/3v2g5c option means the atom list is "v" for the first three supplementary points, then changes to "g" when the next 2 points are added, and reduces to "c" for the final 5 points. Similarly, the 10/2v2g6c option indicates "v" for the first 2, "g" for next 2, and "c" for the final six supplementary points. The standard option,[51] which uses full electronic structure Hessians for all 10 supplementary points, is labeled 10/10a in the present study. The MCMM calculations with the above three options are named MCMM-10/3v2g5c, MCMM-10/2v2g6c, and MCMM-10/10a, respectively. (MCMM-10/10a is equivalent to MCMM-10 in ref 51) We note that, in this article, for all three of the options that are presented, the full electronic structure Hessians are used for the saddle points.

The Hessian elements that are not evaluated by electronic structure calculations are approximated in two ways: (1) from the corresponding values at the saddle point, or (2) from Shepard interpolations in the preceding MCMM calculation, i.e., using the predicted values from an MCMM-α calculation for the next (α + 1)th supplemental point. We applied the first approximation in MCMM-1 employed the second approach in MCMM-*N* with $N > 1$.

We should note that all energies and gradients at Shepard points are determined by electronic structure calculations in the present improved scheme. However, since they are much less expensive than the Hessian to evaluate, such a strategy will not significantly affect the overall computational cost.

## 3. Computational Details and Results

The new strategy for Hessians is tested using the six hydrogen transfer reactions mentioned in section 1. These reactions differ from one another in significant ways (number of atoms,classical barrier height, energy of reaction, saddle point asymmetry, and type and extent of tunneling), and together they provide a challenging test suite.

All electronic structure calculations here (and in the dynamics calculations below) were performed at the MPW1K/6-31+G(d,p)[20] level of theory using GAUSSIAN98 software.[108] MPW1K[20] is a hybrid Hartree−Fock−density functional method[15] that was determined by optimization against a database of barrier heights and reaction energies for 20 reactions. It should be noted that the MPW1K method has been updated in the GAUSSIAN98 package a.11 and later versions based on the corrections indicated in the Appendix of ref 109. The update leads to some small changes in the results[51] for the reactions that were presented previously (R-1 through R-5). The changes are only quantitative and are never qualitative. All electronic structure calculations in this work (both direct dynamics and MCMM) made use of the updated version. We employed spin-restricted wave functions for closed-shell systems (any systems with an even number of electrons) and spin-unrestricted wave functions for open-shell systems.

Table 1 lists the key energetic parameters for the reactive systems investigated here as determined from electronic structure calculations. Table 2 shows geometric information (at the saddle point, denoted ‡, at reactant, R, and at product, P) for the three atoms A−H−B that are directly involved in the hydrogen atom transfer: bond angle $\theta^{\ddagger}_{AHB}$, distances $r^{\ddagger}_{AH}$ and $r^{\ddagger}_{BH}$, and the equilibrium bond distances $r^{P}_{AH}$ and $r^{R}_{BH}$, respectively.

For the conventional and generalized transition states of reactions R-2 to R-6, no low-lying electronically excited states were considered, so the electronic partition of the transition states of these reactions is the ground state degeneracy. For reaction R-1, we explicitly included only the ground triplet state of the transition states but treated it as having a degeneracy of 6 to account for the fact that there are two low-lying triplet electronic states that are nearly degenerate. We included the following electronic excited states in calculating the reactant partition functions:[110] the $^2\Pi_{1/2}$ excited state of OH with an excitation energy of 140 $cm^{-1}$ and the $^3P_1$ and $^3P_0$ excited states

**TABLE 1: Energetic Quantities (kcal/mol) and 0 K Dynamical Bottleneck Locations (bohrs) in the Direct Dynamics Calculations[a]**

| reaction | $V^{\ddagger}$ | $V^{P}$ | $V_{int}^{\ddagger}$ | $V_a^{RG}$ | $V_a^{PG}$ | $V_a^{\ddagger G}$ | $V_a^{AG}$ | $s_*^{AG}$ | $E_{rep}$ (300 K) |
|---|---|---|---|---|---|---|---|---|---|
| $O + CH_4 \rightarrow OH + CH_3$ | 14.02 | 7.83 | 6.20 | 28.85 | 32.56 | 39.30 | 39.33 | −0.032 | 35.86 |
| $HO + CH_4 \rightarrow H_2O + CH_3$ | 7.57 | −9.06 | 7.57 | 34.41 | 24.05 | 40.36 | 41.44 | −0.277 | 40.62 |
| $NH_2 + CH_4 \rightarrow NH_3 + CH_3$ | 13.95 | −1.96 | 13.95 | 41.25 | 39.52 | 54.98 | 54.98 | −0.007 | 48.41 |
| $CH_2F + CH_3Cl \rightarrow CH_3F + CH_2Cl$ | 15.87 | −1.32 | 15.87 | 40.46 | 38.85 | 55.08 | 55.08 | 0.002 | 52.19 |
| $HO + C_3H_8 \rightarrow H_2O + CH_3CHCH_3$ | 2.87 | −16.50 | 2.87 | 72.20 | 54.23 | 73.75 | 74.75 | −0.569 | 74.75 |
| $HO + C_3H_8 \rightarrow H_2O + CH_2CH_2CH_3$ | 4.91 | −12.61 | 4.91 | 72.20 | 58.31 | 75.29 | 76.58 | −0.386 | 76.58 |

[a] All values in this table calculated by MPW1K/6-31+G(d,p). The zero of energy for each reaction is set to the classical potential energy at reactants ($V^{R} \equiv 0$), $V^{\ddagger}$ is the potential energy at the saddle point (equal to classical forward barrier height), $V^{P}$ is the potential energy at the products (equal to classical energy of reaction), $V_{int}^{\ddagger}$ is the intrinsic barrier height, $V_a^{RG}$ is the vibrationally adiabatic ground-state potential energy curve at reactants, and the value of this curve is $V_a^{PG}$ at products, $V_a^{\ddagger G}$ at the saddle point, and $V_a^{AG}$ at the variational transition state (dynamical bottleneck) at 0 K. The representative tunneling energy at 300 K is given as $E_{rep}$ (300 K), $s_*^{AG}$ (in bohr) is the reaction coordinate at the dynamical bottleneck at 0 K. The MCMM calculations exactly reproduce the first six quantities in each row, but give slightly different values, in some cases, for the last three.

**TABLE 2: Geometries for Atoms Directly Involved in Hydrogen Transfer[a]**

| reaction | $\theta_{AHB}^{\ddagger}$ | $r_{AH}^{\ddagger}$ | $r_{BH}^{\ddagger}$ | $r_{AH}^{P}$ [b] | $r_{AH}^{\ddagger} - r_{AH}^{P}$ | $r_{BH}^{R}$ [c] | $r_{BH}^{\ddagger} - r_{BH}^{R}$ |
|---|---|---|---|---|---|---|---|
| $O + CH_4 \rightarrow OH + CH_3$ | 179.2 | 1.184 | 1.306 | 0.966 | 0.218 | 1.086 | 0.220 |
| $HO + CH_4 \rightarrow H_2O + CH_3$ | 173.8 | 1.278 | 1.221 | 0.953 | 0.325 | 1.086 | 0.135 |
| $NH_2 + CH_4 \rightarrow NH_3 + CH_3$ | 171.2 | 1.261 | 1.306 | 1.006 | 0.255 | 1.086 | 0.220 |
| $CH_2F + CH_3Cl \rightarrow CH_3F + CH_2Cl$ | 177.5 | 1.337 | 1.335 | 1.087 | 0.250 | 1.083 | 0.252 |
| $HO + C_3H_8 \rightarrow H_2O + CH_3CHCH_3$ | 176.9 | 1.407 | 1.171 | 0.953 | 0.454 | 1.091 | 0.080 |
| $HO + C_3H_8 \rightarrow H_2O + CH_2CH_2CH_3$ | 177.2 | 1.337 | 1.195 | 0.953 | 0.384 | 1.089 | 0.106 |

[a] All values in this table calculated by MPW1K/6-31+G(d,p). Bond angles in degrees, distances in angstroms. The hydrogen atom is transferred from B to A. Bond angle $\theta_{AHB}^{\ddagger}$, distance $r_{AH}^{\ddagger}$, and distance $r_{BH}^{\ddagger}$ are at the saddle point. [b] Distance $r_{AH}^{P}$ is the equilibrium A−H distance in the product. [c] Distance $r_{BH}^{P}$ is the equilibrium B−H distance in the reactant.

**TABLE 3: Rate Constants ($cm^3$ $Molecule^{-1}$ $s^{-1}$) at 300, 400, and 600 K for the Hydrogen-Transfer Reaction of O with $CH_4$ by Direct Dynamics (DD) and MCMM-10[a]**

| $T$ (K) | TST | CVT | CVT/ZCT | CVT/SCT | CVT/LCT(0) | CVT/LCT | CVT/$\mu$OMT |
|---|---|---|---|---|---|---|---|
| | | | | DD[b] | | | |
| 300 | 5.98E−19 | 5.67E−19 | 1.15E−18 | 1.90E−18 | 6.91E−18 | 6.91E−18 | 6.92E−18 |
| 400 | 5.31E−17 | 5.10E−17 | 7.67E−17 | 1.03E−16 | 1.99E−16 | 1.99E−16 | 2.00E−16 |
| 600 | 6.09E−15 | 5.91E−15 | 7.12E−15 | 8.13E−15 | 1.07E−14 | 1.07E−14 | 1.07E−14 |
| | | | | MCMM-10/10a[c] | | | |
| 300 | 5.98E−19 | 5.98E−19 | 1.14E−18 | 1.85E−18 | 6.48E−18 | 6.48E−18 | 6.48E−18 |
| 400 | 5.31E−17 | 5.31E−17 | 7.68E−17 | 1.02E−16 | 1.92E−16 | 1.92E−16 | 1.92E−16 |
| 600 | 6.09E−15 | 6.05E−15 | 6.92E−15 | 7.93E−15 | 1.05E−14 | 1.05E−14 | 1.05E−14 |
| | | | | MCMM-10/3v2g5c[d] | | | |
| 300 | 5.98E−19 | 5.98E−19 | 1.15E−18 | 1.87E−18 | 6.46E−18 | 6.46E−18 | 6.46E−18 |
| 400 | 5.31E−17 | 5.31E−17 | 7.71E−17 | 1.03E−16 | 1.91E−16 | 1.91E−16 | 1.91E−16 |
| 600 | 6.09E−15 | 6.05E−15 | 6.94E−15 | 7.96E−15 | 1.05E−14 | 1.05E−14 | 1.05E−14 |
| | | | | MCMM-10/2v2g6c[e] | | | |
| 300 | 5.98E−19 | 5.98E−19 | 1.16E−18 | 1.93E−18 | 7.71E−18 | 8.41E−18 | 8.42E−18 |
| 400 | 5.31E−17 | 5.31E−17 | 7.74E−17 | 1.05E−16 | 2.04E−16 | 2.17E−16 | 2.17E−16 |
| 600 | 6.09E−15 | 6.05E−15 | 6.95E−15 | 8.02E−15 | 1.06E−14 | 1.09E−14 | 1.09E−14 |

[a] The rate constant including tunneling is then given by $k^{CVT/MT} = \kappa^{MT} k^{CVT}$, where $\kappa^{MT}$ is the transmission coefficient (denoted $\kappa^{CVT/MT}$ in ref 1), and MT is ZCT, SCT, LCT(0), LCT, or $\mu$OMT. The definition for the transmission coefficient is given in ref 1. See section 2.3 of text for MCMM notation. [b] With $n_{max} = 0$, where $n_{max}$ is the highest vibrational quantum number included in LCT calculations; for direct dynamics, it is the number of energetically allowed final states. [c] With $n_{max} = 0$; the $n_{max}$ for MCMM is determined according to the protocol described in section 3.2 of text. Note that in direct dynamics and MCMM, the potential energy surfaces and reaction paths are not identical, and thus the energetically allowed highest excited states are not necessarily the same. [d] With $n_{max} = 0$. [e] With $n_{max} = 1$.

of $O(^3P)$ with excitation energies of 158 and 227 $cm^{-1}$, respectively.

Both direct dynamics and MCMM calculations were performed. The methodology is documented in ref 51, and here we only describe the aspects most relevant to the present work. We use redundant internal coordinates to represent low-order expansions of potential energy surfaces in internal coordinates.[111−113]

The harmonic approximation was assumed in all cases, and the vibrational analyses were carried out using redundant internal coordinates. For reactions R-1 to R-5, the internal coordinates used here are identical to those used previously.[51] For reaction R-6 they are specified in footnote *a* of Table 8. The current choice of internal coordinates used in vibrational generalized normal-mode analysis yields a reaction-path Hamiltonian with all frequencies real along the computationally kinetically significant ranges of the MEP.

It is well-known that rate constants calculated at low temperatures can be very sensitive to the frequencies of low-frequency vibrational modes. For an almost flat vibrational potential, the use of harmonic-oscillator partition functions based on a very low frequency (e.g., 5 $cm^{-1}$) of a normal mode or

**TABLE 4: Rate Constants ($cm^3$ $molecule^{-1}$ $s^{-1}$) at 300, 400, and 600 K for the Hydrogen-transfer Reaction of OH with $CH_4$ by Direct Dynamics (DD) and MCMM-10[a]**

| *T* (K) | TST | CVT | CVT/ZCT | CVT/SCT | CVT/LCT(0) | CVT/LCT | CVT/$\mu$OMT |
|---|---|---|---|---|---|---|---|
| | | | | DD[b] | | | |
| 300 | 1.26E−15 | 2.59E−16 | 4.84E−16 | 7.64E−16 | 5.39E−16 | 6.23E−16 | 7.65E−16 |
| 400 | 1.69E−14 | 5.36E−15 | 7.55E−15 | 9.87E−15 | 7.90E−15 | 8.64E−15 | 9.88E−15 |
| 600 | 3.00E−13 | 1.39E−13 | 1.59E−13 | 1.80E−13 | 1.62E−13 | 1.69E−13 | 1.80E−13 |
| | | | | MCMM-10/10a[c] | | | |
| 300 | 1.26E−15 | 1.60E−16 | 3.95E−16 | 6.33E−16 | 4.39E−16 | 5.21E−16 | 6.44E−16 |
| 400 | 1.69E−14 | 3.65E−15 | 6.17E−15 | 8.23E−15 | 6.45E−15 | 7.17E−15 | 8.29E−15 |
| 600 | 3.00E−13 | 1.04E−13 | 1.32E−13 | 1.52E−13 | 1.34E−13 | 1.41E−13 | 1.52E−13 |
| | | | | MCMM-10/3v2g5c[d] | | | |
| 300 | 1.26E−15 | 1.57E−16 | 3.89E−16 | 6.13E−16 | 4.31E−16 | 5.76E−16 | 6.59E−16 |
| 400 | 1.69E−14 | 3.61E−15 | 6.10E−15 | 8.04E−15 | 6.37E−15 | 7.78E−15 | 8.52E−15 |
| 600 | 3.00E−13 | 1.04E−13 | 1.31E−13 | 1.50E−13 | 1.33E−13 | 1.48E−13 | 1.55E−13 |
| | | | | MCMM-10/2v2g6c[e] | | | |
| 300 | 1.26E−15 | 1.57E−16 | 3.88E−16 | 6.45E−16 | 4.38E−16 | 6.36E−16 | 7.28E−16 |
| 400 | 1.69E−14 | 3.61E−15 | 6.04E−15 | 8.20E−15 | 6.32E−15 | 8.23E−15 | 9.00E−15 |
| 600 | 3.00E−13 | 1.04E−13 | 1.30E−13 | 1.50E−13 | 1.32E−13 | 1.52E−13 | 1.59E−13 |

[a] See footnotes of Table 3 and section 2.3 of text for notation. [b] With $n_{max} = 1$. [c] With $n_{max} = 1$. [d] With $n_{max} = 2$. [e] With $n_{max} = 2$.

**TABLE 5: Rate Constants ($cm^3$ $molecule^{-1}$ $s^{-1}$) at 300, 400, and 600 K for the Hydrogen-transfer Reaction of $NH_2$ with $CH_4$ by Direct Dynamics (DD) and MCMM-10[a]**

| *T* (K) | TST | CVT | CVT/ZCT | CVT/SCT | CVT/LCT(0) | CVT/LCT | CVT/$\mu$OMT |
|---|---|---|---|---|---|---|---|
| | | | | DD[b] | | | |
| 300 | 6.21E−22 | 6.18E−22 | 3.21E−21 | 7.57E−21 | 1.70E−20 | 1.70E−20 | 1.77E−20 |
| 400 | 2.07E−19 | 2.06E−19 | 5.41E−19 | 8.65E−19 | 1.08E−18 | 1.08E−18 | 1.16E−18 |
| 600 | 9.33E−17 | 9.28E−17 | 1.45E−16 | 1.78E−16 | 1.81E−16 | 1.81E−16 | 1.91E−16 |
| | | | | MCMM-10/10a[c] | | | |
| 300 | 6.21E−22 | 5.73E−22 | 2.42E−21 | 5.97E−21 | 1.72E−20 | 1.73E−20 | 1.81E−20 |
| 400 | 2.07E−19 | 1.91E−19 | 4.36E−19 | 7.25E−19 | 1.01E−18 | 1.01E−18 | 1.11E−18 |
| 600 | 9.33E−17 | 8.50E−17 | 1.22E−16 | 1.53E−16 | 1.59E−16 | 1.59E−16 | 1.72E−16 |
| | | | | MCMM-10/3v2g5c[d] | | | |
| 300 | 6.21E−22 | 5.75E−22 | 2.57E−21 | 6.54E−21 | 1.80E−20 | 1.80E−20 | 1.90E−20 |
| 400 | 2.07E−19 | 1.92E−19 | 4.60E−19 | 7.91E−19 | 1.05E−18 | 1.05E−18 | 1.17E−18 |
| 600 | 9.33E−17 | 8.59E−17 | 1.28E−16 | 1.65E−16 | 1.65E−16 | 1.66E−16 | 1.83E−16 |
| | | | | MCMM-10/2v2g6c[e] | | | |
| 300 | 6.21E−22 | 5.76E−22 | 2.61E−21 | 6.53E−21 | 1.72E−20 | 1.73E−20 | 1.82E−20 |
| 400 | 2.07E−19 | 1.93E−19 | 4.66E−19 | 7.92E−19 | 1.03E−18 | 1.03E−18 | 1.14E−18 |
| 600 | 9.33E−17 | 8.65E−17 | 1.30E−16 | 1.66E−16 | 1.67E−16 | 1.67E−16 | 1.84E−16 |

[a] See footnotes of Table 3 and section 2.3 of text for notation. [b] With $n_{max} = 2$. [c] With $n_{max} = 2$. [d] With $n_{max} = 2$. [e] With $n_{max} = 1$.

**TABLE 6: Rate Constants ($cm^3$ $molecule^{-1}$ $s^{-1}$) at 300, 400, and 600 K for the Hydrogen-Transfer Reaction of $CH_2F$ with $CH_3Cl$ by Direct Dynamics (DD) and MCMM-10[a]**

| *T* (K) | TST | CVT | CVT/ZCT | CVT/SCT | CVT/LCT(0) | CVT/LCT | CVT/$\mu$OMT |
|---|---|---|---|---|---|---|---|
| | | | | DD[b] | | | |
| 300 | 5.45E−24 | 5.44E−24 | 4.94E−23 | 1.19E−22 | 2.24E−22 | 2.24E−22 | 2.40E−22 |
| 400 | 3.48E−21 | 3.48E−21 | 1.27E−20 | 2.08E−20 | 2.15E−20 | 2.15E−20 | 2.41E−20 |
| 600 | 3.08E−18 | 3.07E−18 | 5.57E−18 | 6.91E−18 | 6.51E−18 | 6.51E−18 | 7.07E−18 |
| | | | | MCMM-10/10a[c] | | | |
| 300 | 5.45E−24 | 5.44E−24 | 4.65E−23 | 1.26E−22 | 2.85E−22 | 2.85E−22 | 3.12E−22 |
| 400 | 3.48E−21 | 3.48E−21 | 1.24E−20 | 2.25E−20 | 2.34E−20 | 2.34E−20 | 2.79E−20 |
| 600 | 3.08E−18 | 3.08E−18 | 5.54E−18 | 7.38E−18 | 6.70E−18 | 6.70E−18 | 7.68E−18 |
| | | | | MCMM-10/3v2g5c[d] | | | |
| 300 | 5.45E−24 | 5.44E−24 | 5.27E−23 | 1.76E−22 | 2.89E−22 | 2.89E−22 | 3.41E−22 |
| 400 | 3.48E−21 | 3.48E−21 | 1.37E−20 | 2.94E−20 | 2.45E−20 | 2.45E−20 | 3.29E−20 |
| 600 | 3.08E−18 | 3.08E−18 | 5.90E−18 | 8.72E−18 | 7.10E−18 | 7.10E−18 | 8.88E−18 |
| | | | | MCMM-10/2v2g6c[e] | | | |
| 300 | 5.45E−24 | 5.44E−24 | 5.27E−23 | 1.75E−22 | 2.66E−22 | 2.66E−22 | 3.19E−22 |
| 400 | 3.48E−21 | 3.48E−21 | 1.37E−20 | 2.93E−20 | 2.38E−20 | 2.38E−20 | 3.22E−20 |
| 600 | 3.08E−18 | 3.08E−18 | 5.90E−18 | 8.70E−18 | 7.06E−18 | 7.06E−18 | 8.83E−18 |

[a] See footnotes of Table 3 and section 2.3 of text for notation. [b] With $n_{max} = 1$. [c] With $n_{max} = 1$. [d] With $n_{max} = 1$. [e] With $n_{max} = 1$.

generalized normal mode is unrealistic. To improve the description of generalized normal mode vibrations along the MEP, a frequency cutoff (FC) was introduced in this work. In this treatment, a cutoff value is used instead of the value determined from normal mode or generalized normal-mode analysis if the determined value is smaller. (We note that this has nothing to do with how the PES was obtained; such a cutoff is applied in both direct dynamics and MCMM, and should probably be

**TABLE 7: Rate Constants ($cm^3$ $molecule^{-1}$ $s^{-1}$) at 300, 400, and 600 K for the Hydrogen-Transfer Reaction of OH with $C_3H_8$ at the Secondary Position by Direct Dynamics (DD) and MCMM-10[a]**

| *T* (K) | TST | CVT | CVT/ZCT | CVT/SCT | CVT/LCT(0) | CVT/LCT | CVT/$\mu$OMT |
|---|---|---|---|---|---|---|---|
| | | | | DD[b] | | | |
| 300 | 1.85E−13 | 4.65E−14 | 4.86E−14 | 4.90E−14 | 4.86E−14 | 4.91E−14 | 4.92E−14 |
| 400 | 4.64E−13 | 1.76E−13 | 1.70E−13 | 1.71E−13 | 1.70E−13 | 1.71E−13 | 1.71E−13 |
| 600 | 1.53E−12 | 8.36E−13 | 7.84E−13 | 7.86E−13 | 7.85E−13 | 7.86E−13 | 7.87E−13 |
| | | | | MCMM-10/10a[c] | | | |
| 300 | 1.85E−13 | 3.52E−14 | 3.67E−14 | 3.76E−14 | 3.67E−14 | 3.70E−14 | 3.76E−14 |
| 400 | 4.64E−13 | 1.38E−13 | 1.37E−13 | 1.38E−13 | 1.37E−13 | 1.37E−13 | 1.39E−13 |
| 600 | 1.53E−12 | 6.90E−13 | 6.61E−13 | 6.65E−13 | 6.62E−13 | 6.63E−13 | 6.66E−13 |
| | | | | MCMM−10/3v2g5c[d] | | | |
| 300 | 1.85E−13 | 3.46E−14 | 3.69E−14 | 3.81E−14 | 3.69E−14 | 3.70E−14 | 3.81E−14 |
| 400 | 4.64E−13 | 1.37E−13 | 1.37E−13 | 1.39E−13 | 1.37E−13 | 1.37E−13 | 1.39E−13 |
| 600 | 1.53E−12 | 6.90E−13 | 6.59E−13 | 6.64E−13 | 6.59E−13 | 6.59E−13 | 6.64E−13 |
| | | | | MCMM-10/2v2g6c[e] | | | |
| 300 | 1.85E−13 | 3.47E−14 | 4.41E−14 | 4.80E−14 | 4.42E−14 | 4.46E−14 | 4.80E−14 |
| 400 | 4.64E−13 | 1.38E−13 | 1.55E−13 | 1.62E−13 | 1.55E−13 | 1.56E−13 | 1.62E−13 |
| 600 | 1.53E−12 | 7.05E−13 | 7.21E−13 | 7.36E−13 | 7.21E−13 | 7.23E−13 | 7.36E−13 |

[a] See footnotes of Table 3 and section 2.3 of text for notation. [b] With $n_{max} = 2$. [c] With $n_{max} = 2$. [d] With $n_{max} = 1$. [e] With $n_{max} = 1$.

**TABLE 8: Rate Constants ($cm^3$ $molecule^{-1}$ $s^{-1}$) at 300, 400, and 600 K for the Hydrogen-Transfer Reaction of OH with $C_3H_8$ at the Primary Position by Direct Dynamics (DD) and MCMM-10[a]**

| *T* (K) | TST | CVT | CVT/ZCT | CVT/SCT | CVT/LCT(0) | CVT/LCT | CVT/$\mu$OMT |
|---|---|---|---|---|---|---|---|
| | | | | DD[b] | | | |
| 300 | 3.65E−14 | 3.55E−15 | 3.85E−15 | 4.16E−15 | 3.84E−15 | 3.89E−15 | 4.16E−15 |
| 400 | 1.77E−13 | 2.76E−14 | 2.73E−14 | 2.85E−14 | 2.73E−14 | 2.74E−14 | 2.85E−14 |
| 600 | 1.15E−12 | 2.71E−13 | 2.53E−13 | 2.58E−13 | 2.53E−13 | 2.53E−13 | 2.58E−13 |
| | | | | MCMM-10/10a[c] | | | |
| 300 | 3.66E−14 | 1.38E−15 | 2.24E−15 | 2.53E−15 | 2.25E−15 | 2.31E−15 | 2.55E−15 |
| 400 | 1.77E−13 | 1.26E−14 | 1.67E−14 | 1.79E−14 | 1.67E−14 | 1.70E−14 | 1.80E−14 |
| 600 | 1.15E−12 | 1.46E−13 | 1.66E−13 | 1.71E−13 | 1.66E−13 | 1.67E−13 | 1.72E−13 |
| | | | | MCMM-10/3v2g5c[d] | | | |
| 300 | 3.66E−14 | 3.54E−15 | 2.57E−15 | 3.11E−15 | 2.58E−15 | 2.65E−15 | 3.11E−15 |
| 400 | 1.77E−13 | 2.48E−14 | 1.72E−14 | 1.92E−14 | 1.73E−14 | 1.75E−14 | 1.92E−14 |
| 600 | 1.15E−12 | 2.20E−13 | 1.56E−13 | 1.64E−13 | 1.56E−13 | 1.57E−13 | 1.64E−13 |
| | | | | MCMM-10/2v2g6c[e] | | | |
| 300 | 3.66E−14 | 3.60E−15 | 2.64E−15 | 3.25E−15 | 2.65E−15 | 2.73E−15 | 3.26E−15 |
| 400 | 1.77E−13 | 2.53E−14 | 1.75E−14 | 1.97E−14 | 1.76E−14 | 1.79E−14 | 1.97E−14 |
| 600 | 1.15E−12 | 2.23E−13 | 1.58E−13 | 1.66E−13 | 1.58E−13 | 1.59E−13 | 1.66E−13 |

[a] The internal coordinates used in the vibrational analysis of the generalized normal modes along the reaction path are 1-2, 3-2, 4-2, 5-2, 1-2-3, 1-2-4, 1-2-5, 3-2-4, 3-2-5, 4-2-5, 5-8, 5-9, 5-10, 2-5-8, 2-5-9, 2-5-10, 8-5-9, 8-5-10, 9-5-10, 8-11, 8-12, 8-13, 5-8-11, 5-8-12, 5-8-13, 11-8-12, 11-8-13, 12-8-13, 1-2-5-9, 10-5-8-11, 6-7, 6-3, 3-6-7, 2-6-7, 1-2-6, 4-2-6, 5-2-6, 1-2-6-7, 4-2-6-7, 5-2-6-7, 6-2-1-3, 6-2-4-3, 6-2-5-3, 7-6-3-1, 7-6-3-4, 7-6-3-5, 6-7-3-1, and 6-7-3-4, where *X-Y* denotes a bond stretching coordinate, *X-Y-Z* denotes a valence bend, and *W-X-Y-Z* denotes a torsion. See footnotes of Table 3 and section 2.3 of text for other notation. [b] With $n_{max} = 2$. [c] With $n_{max} = 1$. [d] With $n_{max} = 1$. [e] With $n_{max} = 1$.

applied even with realistic analytic PESs. It corrects the breakdown of the harmonic approximation, not the breakdown of MCMM.)

In the present work, the FC was set to 10 $cm^{-1}$ for all reactions. This value is arbitrary and probably too conservative, i.e., too small, but it appears to be a reasonable choice. Moreover, we have tested two other FC values, 5 and 15 $cm^{-1}$, for reaction R-6, which has a very low-frequency mode (the MEP range that is close to the bottleneck regions with all frequencies equal to or higher than 15 $cm^{-1}$ is as follows: $-0.35$ $a_0 < s < 0.00$ $a_0$ and $0.10$ $a_0 < s < 0.65$ $a_0$). The results with FC = 15 $cm^{-1}$ are presented in Table 9 and those for FC = 5 $cm^{-1}$ are in the Supporting Information (Table S-8). Only minor changes (usually less than 5%) are found to the reaction rates including LCT rates. For the other reactions, the frequencies of normal modes are larger than 15 $cm^{-1}$ along very long ranges of the MEP (e.g. $-0.80$ $a_0 < s < 1.90$ $a_0$ for R-4, and $-2.00$ $a_0 < s < 0.80$ $a_0$ for R-5), and the effects on the reaction rates due to the present selection of FC value are therefore expected to be insignificant.

**3.1. Direct Dynamics.** The direct dynamics calculations were carried out using GAUSSRATE,[114] which is an interface of POLYRATE[115] with GAUSSIAN.[108] We modified the GAUSSRATE package by inclusion of a low-frequency cutoff (will be addressed later in this section).

As in our previous study,[51] the Page−McIver method[116] was chosen to follow the MEP in isoinertial coordinates. The coordinates were scaled to a reduced mass $\mu$ of 1 amu. A step size of 0.005 $a_0$ was used for the gradient, and a new Hessian was calculated every 0.05 $a_0$ along the MEP. The reaction path was calculated out to 2.0 to 4.0 $a_0$ on the high side and to 2.0 to 3.0 $a_0$ on the low side. This is sufficient to converge the zero-curvature tunneling (ZCT),[1,8,97] SCT, LCT(0), LCT, and microcanonical optimized multidimensional tunneling ($\mu$OMT)[8,36] calculations. LCT and $\mu$OMT calculations include tunneling into vibrationally excited states, to the extent that it occurs, and LCT(0) stands for tunneling only into ground state.

For the six reactions studied here, the contribution from large-curvature tunneling into an excited state is found to be rather small, and it decreases dramatically toward negligible as the

**TABLE 9: Rate Constants ($cm^3$ $molecule^{-1}$ $s^{-1}$) at 300, 400, and 600 K for the Hydrogen-Transfer Reaction of OH with $C_3H_8$ at the Primary Position by Direct Dynamics (DD) and MCMM-10 with Frequency Cutoff (FC) Set to 15 $cm^{-1}$[a]**

| *T* (K) | TST | CVT | CVT/ZCT | CVT/SCT | CVT/LCT(0) | CVT/LCT | CVT/$\mu$OMT |
|---|---|---|---|---|---|---|---|
| | | | | DD[b] | | | |
| 300 | 3.65E−14 | 3.55E−15 | 3.83E−15 | 4.14E−15 | 3.82E−15 | 3.87E−15 | 4.14E−15 |
| 400 | 1.77E−13 | 2.76E−14 | 2.72E−14 | 2.84E−14 | 2.72E−14 | 2.73E−14 | 2.84E−14 |
| 600 | 1.15E−12 | 2.71E−13 | 2.52E−13 | 2.57E−13 | 2.52E−13 | 2.53E−13 | 2.57E−13 |
| | | | | MCMM-10/10a[c] | | | |
| 300 | 3.66E−14 | 1.38E−15 | 2.23E−15 | 2.51E−15 | 2.24E−15 | 2.30E−15 | 2.53E−15 |
| 400 | 1.77E−13 | 1.26E−14 | 1.66E−14 | 1.78E−14 | 1.67E−14 | 1.70E−14 | 1.79E−14 |
| 600 | 1.15E−12 | 1.46E−13 | 1.66E−13 | 1.71E−13 | 1.66E−13 | 1.67E−13 | 1.71E−13 |
| | | | | MCMM-10/3v2g5c[d] | | | |
| 300 | 3.66E−14 | 3.54E−15 | 2.54E−15 | 3.06E−15 | 2.54E−15 | 2.61E−15 | 3.06E−15 |
| 400 | 1.77E−13 | 2.48E−14 | 1.71E−14 | 1.90E−14 | 1.71E−14 | 1.74E−14 | 1.90E−14 |
| 600 | 1.15E−12 | 2.20E−13 | 1.55E−13 | 1.63E−13 | 1.55E−13 | 1.56E−13 | 1.63E−13 |
| | | | | MCMM-10/2v2g6c[e] | | | |
| 300 | 3.66E−14 | 3.60E−15 | 2.60E−15 | 3.21E−15 | 2.62E−15 | 2.70E−15 | 3.21E−15 |
| 400 | 1.77E−13 | 2.53E−14 | 1.73E−14 | 1.95E−14 | 1.74E−14 | 1.77E−14 | 1.95E−14 |
| 600 | 1.15E−12 | 2.23E−13 | 1.57E−13 | 1.65E−13 | 1.57E−13 | 1.58E−13 | 1.65E−13 |

[a] See footnotes of Table 3 and section 2.3 of text for notation. [b] With $n_{max} = 2$. [c] With $n_{max} = 1$. [d] With $n_{max} = 1$. [e] With $n_{max} = 1$.

excitation increases; however, it would not be known that this is the case without doing the numerical calculations, and therefore it is important to show that MCMM does not overestimate LCT including all possible final states.

**3.2. MCMM Dynamics.** The MCMM dynamics calculations were carried out using the MC-TINKERATE[117] program, which is a new development based upon the TINKERATE[118] program that was used in previous studies.[51] MC-TINKERATE is an interface between the POLYRATE[115] and MC-TINKER,[119] and MC-TINKER is an enhanced version of TINKER.[120] The Shepard interpolations were carried out by MC-TINKER, and molecular mechanics calculations were carried out with TINKER. The parameters for the molecular mechanics force field are those of the MM3 force field[22−24] installed in TINKER plus a few parameters defined in ref 51. Three options (10/3v2g5c, 10/2v2g6c, and 10/10a) are compared. For reactions R-1 to R-4, options 10/3v2g5c and 10/2v2g6c simplify to 10/5g5c and 10/6g4c, respectively, since there are only geminal and core atoms in these systems.

The treatment to the reaction path (the method to follow the MEP, the choice of internal coordinates for generalized normal-mode analysis, etc.) is the same as in direct dynamics calculations except as follows:

(1) We adopted a finer step size of 0.001 $a_0$ for the gradient and 0.01 $a_0$ for the Hessian along the MEP,[121] since MCMM calculations are much less expensive.

(2) We chose a narrower *s* range in the MCMM calculations in some cases. This is because, with a small number of electronic structure data, the MCMM calculations over wide *s* ranges sometimes show unphysical behavior in ranges where the MCMM method is not yet converged. However, such very wide reaction paths are not needed for reasonably well converged VTST/$\mu$OMT calculations.

(3) Tunneling may occur in MCMM calculations into higher excited states than in direct dynamics studies. Tunneling paths of some highly excited states lie outside the concave side regions that are well-defined in MCMM-10. Consequently, one obtains large LCT rates, but that is an artifact. To eliminate this artifact without making use of the direct dynamics results (so as to provide a test of the methodology that is relevant to the practical situation where the direct dynamics results are not know), we adopted a prespecified protocol for how many final states to include in the LCT calculation; in particular, we successively increased the vibrational quantum number of the highest excited state considered in LCT until the tunneling contribution is converged within 1% or until the contribution from the newly added state reaches a local minimum (with respect to vibrational quantum number), whichever happens first. Reasonable LCT rates were achieved by doing so. The highest vibrational quantum numbers included in the MCMM calculations according to this scheme are given for reactions R-1 to R-6, respectively, in the footnotes of Tables 3−9, where they are compared to the values used in the direct dynamics calculations.

The locations of the supplementary points were determined according to the standard scheme, which is explained in ref 51 and is reviewed in Table S-1 of the Supporting Information. They are collected in Table S-9 of the Supporting Information. For the eighth to the tenth supplementary points, we showed instead the locations of corresponding assistant points ($8_H/8_L$, $9_H/9_L$, and $10_H/10_L$). For comparison, we also listed the locations for reactions R-1 to R-5 as determined in ref 51 using the old MPW1K (note that reactions R-1 to R-5 in this work correspond respectively to reactions R-2 to R-6 in ref 51, and MCMM-10/10a here is identical to MCMM-10 in ref 51).

As a technical detail, we note that most electronic structure programs only have an option to calculate the whole Hessian. However, to reap the advantages of the new method, one needs to calculate only the elements that one uses, according to the procedure described in section 2.3. In practical work on large systems where the Hessians are obtained by numerical differentiation of gradients, one would numerically compute only the elements that are needed for the MCMM calculations.

**3.3. Results.** Encouragingly, we found that the *s* values for the first 7 supplementary points, which are located on MEP, usually do not change much (typically less than 0.03 $a_0$) between MCMM-10/10a, MCMM-10/3v2g5c, and MCMM-10/2v2g6c. The assistant points show larger deviations, especially for those reactions having very low barriers, e.g., R-5 (2.9 kcal/mol) and R-6 (4.9 kcal/mol). This is expected because the assistant points are determined according to $V_a^G$, which is sensitive to the frequencies of generalized normal modes. However, we found that the LCT results are not very sensitive to such variations in assistant point locations.

Furthermore, it is evident that the update of MPW1K only introduces minor changes to the locations, as only small differences are detected between MCMM-10(/10a) in this work that used the updated MPW1K and in ref 51 that used the old MPW1K. These small changes of the locations for the supple-

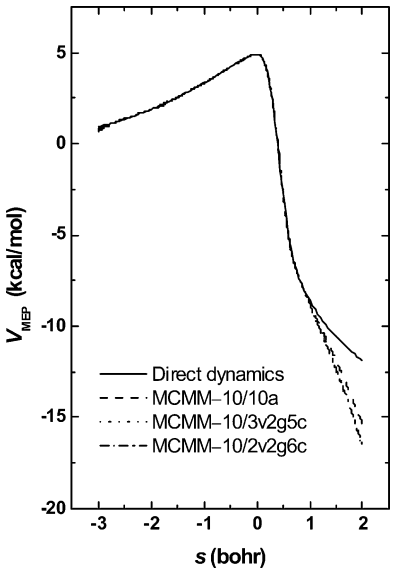


**Figure 4.** Potential energies along the MEP for OH + $C_3H_8 \rightarrow H_2O + CH_2CH_2CH_3$. The MCMM-10/3v2g5c and MCMM-10/2v2g6c curves are superimposable to plotting accuracy.

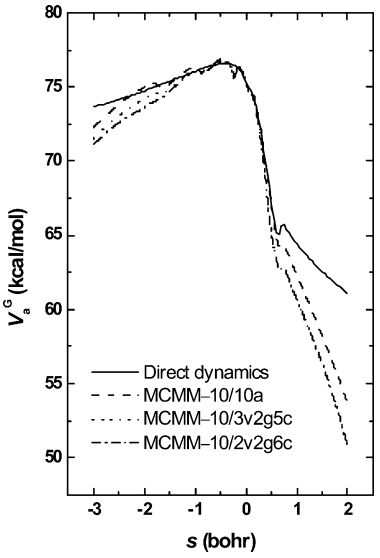


**Figure 5.** Vibrationally adiabatic ground-state energies along the MEP for OH + $C_3H_8 \rightarrow H_2O + CH_2CH_2CH_3$.

mentary points imply that the current practical scheme of locating supplementary points is robust.

Reaction path profiles for reaction R-6, which is newly introduced in the present paper into the test suite, are illustrated in Figures 4 and 5 for the potential energies and vibrationally adiabatic ground-state energies, respectively; furthermore, the locations of the supplementary Shepard points are illustrated in Figure 6. The calculated reaction rates for R-1 to R-6 are tabulated for 300, 400, and 600 K in Tables 3−8, respectively. Results for additional temperatures are given in Tables S-2 to S-7 of the Supporting Information.

## 4. Discussion

Tables 3−9 show that the reaction rates given by MCMM agree well with direct dynamics calculations. The key result of the present article is that the errors of the MCMM-10/3v2g5c and MCMM-10/2v2g6c calculations are comparable to MCMM-10/10a. The extent of the agreement varies from one reaction to another. For example, MCMM-10/10a using full electronic-

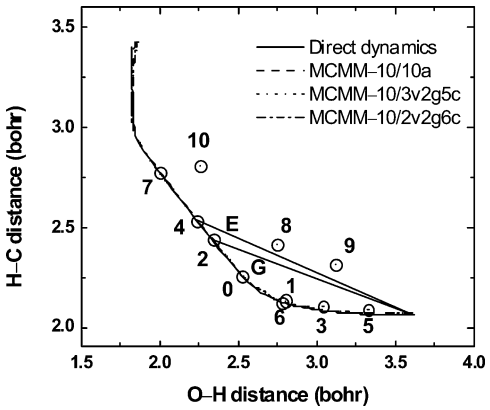


**Figure 6.** Two-dimensional representations of the reaction paths ($-2.0\ a_0 < s < +3.0\ a_0$) given by direct dynamics and MCMM-10 for reaction OH + $C_3H_8 \rightarrow H_2O + CH_2CH_2CH_3$. The saddle and supplementary points used in MCMM-10/10a are shown. Two straight lines illustrate the direct dynamics tunneling paths, respectively, into the ground state (G) and into the first vibrationally excited state (E) at $V_a^G(s)$ equal to $(V_a^{HG} + V_a^{\ddagger G})/2$.

**TABLE 10: Bottleneck Properties at 300 K for the Hydrogen-Transfer Reaction of OH with $CH_4$ by Direct Dynamics (DD) and MCMM-10/10a[a]**

| | direct dynamics | | MCMM-10/10a | |
|---|---|---|---|---|
| $s_*^{AG}$ | −0.259 | | −0.403 | |
| $V_a^{AG}$ | 41.43 | | 41.66 | |
| $V_{MEP}$ ($s_*^{AG}$) | 6.87 | | 6.36 | |
| $I$ [$Q_{rot}$] | 3.541E+15 | [8.7E+3] | 3.675E+15 | [8.9E+3] |
| $\nu_1$ [$Q_{vib,1}$] | 3911 | [8.5E−5] | 3872 | [9.3E−5] |
| $\nu_2$ [$Q_{vib,2}$] | 3281 | [3.8E−4] | 3291 | [3.7E−4] |
| $\nu_3$ [$Q_{vib,3}$] | 3277 | [3.9E−4] | 3286 | [3.8E−4] |
| $\nu_4$ [$Q_{vib,4}$] | 3152 | [5.2E−4] | 3163 | [5.1E−4] |
| $\nu_5$ [$Q_{vib,5}$] | 2002 | [8.2E−3] | 2476 | [2.6E−4] |
| $\nu_6$ [$Q_{vib,6}$] | 1544 | [2.5E−2] | 1555 | [2.4E−2] |
| $\nu_7$ [$Q_{vib,7}$] | 1515 | [2.7E−2] | 1526 | [2.6E−2] |
| $\nu_8$ [$Q_{vib,8}$] | 1393 | [3.5E−2] | 1398 | [3.5E−2] |
| $\nu_9$ [$Q_{vib,9}$] | 1335 | [4.1E−2] | 1353 | [3.9E−2] |
| $\nu_{10}$ [$Q_{vib,10}$] | 1275 | [4.7E−2] | 1310 | [4.3E−2] |
| $\nu_{11}$ [$Q_{vib,11}$] | 798 | [1.5E−1] | 765 | [1.6E−1] |
| $\nu_{12}$ [$Q_{vib,12}$] | 328 | [5.7E−1] | 330 | [5.7E−1] |
| $\nu_{13}$ [$Q_{vib,13}$] | 318 | [6.0E−1] | 318 | [6.0E−1] |
| $\nu_{14}$ [$Q_{vib,14}$] | 44 | [4.7E+0] | 50 | [4.2E+0] |
| $Q_{vib}$ | 5.9E−25 | | 1.5E−25 | |

[a] The maximum of the vibrationally adiabatic ground-state potential energy curve is given as $V_a^{AG}$ in kcal/mol, its location along the MEP denotes $s_*^{AG}$ (in bohr), $V_{MEP}$ is the corresponding potential energy (in kcal/mol) on MEP, $I$ is the determinant of the moment of inertia tensor (i.e., the product of the principal moments of inertia) in amu$^3$ bohr$^6$ (1 amu$^3$ bohr$^6$ = 1.0054 × $10^{-142}$ kg$^3$m$^6$), $Q_{rot}$ is the rotational partition function, $\nu_i$ ($i$ = 1, 2, ..., 14) is the $i$th generalized normal mode in cm$^{-1}$, $Q_{vib,i}$ is the vibrational partition function for mode $i$, and $Q_{vib}$ is the total vibrational partition function.

structure Hessians does better for reaction R-4, while MCMM-10/2v2g6c using partial electronic-structure Hessians gives closer agreement for reaction R-5, probably due to error cancellations. If no LCT rates are desired, the intermediate results with six supplementary points (see Table 11), MCMM-6/6a, MCMM-6/3v2g1c, and MCMM-6/2v2g2c, are capable of providing reasonably good rate constants.

We noted that the direct dynamics CVT rates for reactions R-2, R-5, and R-6 are reproduced less satisfactorily by MCMM. These three reactions are highly exothermic reactions with low classical barriers (see Table 1). This means that $V_{MEP}$ is very flat on the reactant side, and it drops quickly on the product side. For each of these three reactions, the locations of the

**TABLE 11: Mean Unsigned Percentage Errors of Reaction Rates for Various MCMM Computations (with Respect to Direct Dynamics) Calculated by Averaging over the Three Temperatures (300, 400, and 600 K) for Six Reactions[a]**

| *T* (K) | CVT | CVT/ZCT | CVT/SCT | CVT/LCT(0) | CVT/LCT | CVT/$\mu$OMT |
|---|---|---|---|---|---|---|
| 10/10a | 19 | 16 | 15 | 16 | 15 | 16 |
| 10/3v2g5c | 12 | 15 | 19 | 16 | 14 | 17 |
| 10/2v2g6c | 11 | 13 | 16 | 13 | 12 | 13 |
| 6/6a | 18 | 15 | 14 | | | |
| 6/3v2g1c | 12 | 15 | 18 | | | |
| 6/2v2g2c | 12 | 13 | 16 | | | |

[a] Six reactions: (1) $O + CH_4 \rightarrow HO + CH_3$, (2) $HO + CH_4 \rightarrow H_2O + CH_3$, (3) $NH_2 + CH_4 \rightarrow NH_3 + CH_3$, (4) $CH_2F + CH_3Cl \rightarrow CH_3F + CH_2Cl$, (5) $HO + C_3H_8 \rightarrow H_2O + CH_3CHCH_3$, (6) $HO + C_3H_8 \rightarrow H_2O + CH_2CH_2CH_3$. See footnotes of Table 3 and section 2.3 of text for explanation of notation.

**TABLE 12: Mean Unsigned Percentage Errors of Reaction Rates for Various MCMM Computations (with Respect to MCMM-10/10a Which Uses Full Electronic Structure Hessians for all 10 Supplementary Shepard Points) Calculated by Averaging over the Three Temperatures (300, 400, and 600 K) for Six Reactions[a]**

| *T* (K) | CVT | CVT/ZCT | CVT/SCT | CVT/LCT(0) | CVT/LCT | CVT/$\mu$OMT |
|---|---|---|---|---|---|---|
| 10/3v2g5c | 17 | 3 | 8 | 2 | 3 | 5 |
| 10/2v2g6c | 17 | 6 | 11 | 6 | 9 | 11 |
| 6/6a | 0 | 1 | 1 | | | |
| 6/3v2g1c | 15 | 4 | 8 | | | |
| 6/2v2g2c | 15 | 6 | 11 | | | |

[a] Six reactions: (1) $O + CH_4 \rightarrow HO + CH_3$, (2) $HO + CH_4 \rightarrow H_2O + CH_3$, (3) $NH_2 + CH_4 \rightarrow NH_3 + CH_3$, (4) $CH_2F + CH_3Cl \rightarrow CH_3F + CH_2Cl$, (5) $HO + C_3H_8 \rightarrow H_2O + CH_3CHCH_3$, (6) $HO + C_3H_8 \rightarrow H_2O + CH_2CH_2CH_3$. See footnotes of Table 3 and section 2.3 of text for explanation of notation.

canonical variational transition states, which happen to be on the reactant side, depend strongly on the frequencies of the generalized normal modes along the MEP, since the $V_{MEP}$ changes slowly over a long range of *s*. Two kinds of generalized normal modes are of particular importance in determining the location and quantized energy levels of the variational transition states; the low frequency modes and the modes strongly coupled to bond-breaking/bond-forming; for these modes the convergence of the frequencies is not as robust as for the other modes. Furthermore, as expected in calculations in which we pushed the interpolation scheme to its limit of very sparse data, there are oscillations in the frequencies of the normal modes along the MCMM reaction paths. The oscillations of the frequencies do not usually affect $V_a^G(s)$ significantly, but they have a larger effect on vibrational partition functions along the MEP, on the location of the bottleneck, and on the value of CVT rate constant. However, the CVT rate constant is simply an intermediate result, and the effect on the final rate constants is smaller than the effect on the CVT ones,[122] so that even for these difficult cases, the rate constants including any of the three kinds of tunneling calculations (ZCT, SCT, or LCT) are well converged.

To further demonstrate the most difficult kind of situation, we take reaction R-2 as an example and list in Table 10 the bottleneck properties at 300 K for both MCMM-10/10a and direct dynamics. One sees that effects due to variations in the moment of inertia (and therefore changes in rotational partition functions) are rather small. The value of $V_{MEP}$ at the maximum of $V_a^G$ decreases by ca. 0.51 kcal/mol in MCMM-10/10a, whereas the value of $V_a^G$ differs by just 0.23 kcal/mol. These kinds of interpolation errors increase the calculated rates, but contributions from vibrational partition functions, especially from the $\nu_5$ mode (the $C^2-H^3-O^6$ bend), act in the opposite direction, giving rise to an overall difference of about a factor of 1.6. The differences between interpolated and direct dynamics CVT rates would eventually vanish with inclusion of more and more supplementary points, but our goal here is to test the method aggressively with very few points. In particular, our emphasis here is to obtain good results for all reactions in our test suite with a single, general scheme using as small an amount of higher-level data as possible, and the general conclusion from the table is that the method is very successful in achieving this goal. Even the errors in CVT rates are still within an acceptable range.

To further assess on the overall performance of the options studied here, the mean unsigned percentage error (MUPE) with respect to direct dynamics is evaluated; this is defined as

$$\mathrm{MUPE} = \left(\frac{1}{N}\sum_{i=1}^{N}\left|\frac{k_i^{\mathrm{MCMM}} - k_i^{\mathrm{DD}}}{k_i^{\mathrm{DD}}}\right|\right) \times 100\% \qquad (9)$$

where $k_i^{\mathrm{MCMM}}$ is the MCMM rate constant, $k_i^{\mathrm{DD}}$ is the direct dynamics result that the MCMM algorithm tries to reproduce, and *N* is the number of rate constants for which the comparisons are made. Although MUPE does not give an even-handed representation of the cases in which the rate constants are underestimated (those cases are limited to a percentage error of 100%), it is very instructive and has been used extensively.

Table 11 lists the MUPE of reaction rates for various MCMM computations (with respect to direct dynamics) calculated by averaging over all three temperatures ($T = 300$, 400, and 600 K) for all six reactions ($N = 18$). It is very encouraging to see that the MUPE values for types of rate calculations that include tunneling are in the range 12−17%, and even the errors in the more sensitive CVT rate constants are in the range 11−19%. This demonstrates the success of using partial electronic structure Hessians in MCMM. Furthermore, the most new significant finding of the present paper is that the MUPE values with partial electronic Hessians are not systematically larger than those with full electronic structure Hessians. Thus, we have succeeded in our objective of decreasing the computational cost by using less Hessian information for atoms remote from the core.

To underscore this point, we show in Table 12 the MUPE for partial-electronic-structure-Hessian MCMM computations with respect to MCMM-10/10a, which uses full electronic structure Hessians for all 10 supplementary Shepard points. MUPE is defined similar to eq 9 but replacing $k_i^{\mathrm{DD}}$ by $k_i^{\mathrm{MCMM\text{-}10/10a}}$. This presents an indication, from another point of

view, of the quality of the partial electronic structure Hessians in MCMM. Again, all MCMM-10/10a rates that include tunneling are reasonably well reproduced by MCMM with partial electronic structure Hessians. As expected, the 10/3v2g5c(6/3v2g1c) option converges to 10/10a(6/6a) better than 10/2v2g6c(6/2v2g2c) does.

The newly developed method to treat the Hessians greatly reduces the computational effort when analytical Hessians are not available, which is not uncommon. In such cases the total cost of the calculation is dominated by the cost of the Hessians.[123] In the standard MCMM scheme, one needs to evaluate full Hessians by carrying out electronic structure calculations for 11 points (including the saddle point and the supplementary points). In the improved scheme, one just does so for certain Hessian elements. Taking reaction R-6 as an example, we can estimate the saving of computational costs. For reaction R-6, one has three core, four geminal, three vicinal, and three distant atoms. In total there are 13 atoms, resulting in a $39 \times 39$ Hessian matrix for which (after taking account of symmetry) 780 unique elements are to be determined. Employing the 10/10a option, one would have to compute $780 \times 11 = 8085$ elements numerically at the level of electronic structure calculations. In contrast, the 3v2g5c option requires only $780 + 3 \times 465 + 2 \times 231 + 5 \times 45 = 2862$ such computations, and 2v2g6c asks for even less, in particular $780 + 2 \times 465 + 2 \times 231 + 6 \times 45 = 2442$ elements. As the methods used to obtain approximate Hessian elements (see section 2.3) have negligible expense compared with the electronic structure calculations, the 3v2g5c and 2v2g6c options reduce the computational effort of Hessian evaluations for reaction R-6 by factors of 2.8 and 3.3, respectively. When the reactive system becomes larger and larger, this factor will eventually converge to 11 since, in the scheme tested here, only the saddle point needs to be treat with full electronic structure Hessians.

The improved MCMM scheme presented here may also be helpful when analytical Hessians are available, if the analytical Hessian computation for the whole system (we are not aware of electronic structure programs that have an option to calculate partial analytic Hessians) is more expensive than the numerical evaluation of Hessian elements for a small set of atoms. We emphasize here, however, that the improved MCMM method is most useful when analytical Hessians are not available. This is especially true when electronic structure calculations at very high level of theories are used. In such a circumstance, the present improvement to the standard MCMM method is particularly attractive since one saves a larger fraction of the computational cost for a bigger system.

It is instructive to compare the present procedure to methods that do not require any gradient or Hessian information. An example is the interpolated moving least-squares method.[124] This method generates the data for Shepard interpolation from moving least-squares calculations. However, if the least-squares steps of this method are to adequately represent quadratic Taylor's series expansions about the expansion centers, they must include a number of points at least equal to the number required to compute gradients and Hessians numerically. The present method then has two key advantages: (1) Much of the required information about how the potential energy changes when the coordinates are changed is supplied by the molecular mechanics potentials, and the electronic structure coordinate grid does not need to extend into coordinates that are well represented by molecular mechanics. (2) The present article has shown that one needs very little Hessian data in spectator degrees of freedom, and it also shows the standard scheme can be modified to allow more information about some coordinates than about others. The lessons learned in the present study about the ability to use partial electronic structure Hessian data could also be utilized to make other Shepard interpolation schemes[104,105,124] more efficient, although in this work we have only explicitly considered the MCMM approach.

## 5. Concluding Remarks

In this work, we improved the efficiency of the standard MCMM method by using partial electronic structure Hessians and treating most of the elements of the Hessians approximately for the supplementary Shepard points. The new MCMM strategy was tested against a diverse test suite of six reactions with up to 13 atoms, and reasonably accurate rate constants were obtained, as demonstrated by comparisons with the standard MCMM strategy employing full electronic structure Hessians and also by comparisons with direct dynamics at the same electronic structure level. This new procedure reduces the computational effort associated with the nonstationary points by a factor of up to 3 for the reactions under investigation, and the savings would be more than an order of magnitude for even larger reactive systems.

The present study makes MCMM more affordable for fitting expensive electronic structure methods applied to medium-size molecules and also makes a promising step toward application of MCMM to very large molecules. However, the practical treatment of very large molecules demands further developments. One of the critical issues will be to improve the treatment for the saddle point, which is handled completely at the electronic structure level in the present schemes. A promising approach is to combine the MCMM method with a combined quantum-mechanics/molecular-mechanics (QM/MM) method that applies quantum mechanics to a subsystem of active atoms and molecular mechanics to the rest[125−131] or with a dual-level method that uses high-level quantum mechanics for active atoms and low-level quantum mechanics for the other atoms.[132−135] (One could also consider using low-level data instead of interpolated data at the nonstationary points.)

In considering the extension of this kind of approach to calculations on very large systems, we also note that vibrational enthalpy and entropy changes can be calculated in some cases on the basis of partial Hessian vibrational analysis.[136−141] Although the present paper uses the full Hessian for vibrational analysis, it is clear that further advantages will accrue if it is combined with a partial Hessian method for large systems.

Although the present article has been concerned with Shepard interpolation of the resonance integral in the context of multiconfiguration molecular mechanics, some methods apply Shepard interpolation directly to the potential energy surface,[104,105,124] and the same kind of savings as achieved here by using partial Hessians could also be achieved in these methods by using partial Hessians.

The MCMM approach presented here is likely to be useful for a large variety of problems, although here we only examined hydrogen abstraction reactions, which provide especially challenging tests of the new method due to significant tunneling and variational effects. It will be interesting to investigate other reactions such as addition or elimination reactions, heavy-atom transfer reactions, and group transfer reactions. In addition to rate constant calculations, it will also be desirable to analyze other problems, e.g., kinetic isotope effects (KIEs), which are very useful in understanding the mechanisms of enzymatic reactions. KIEs are very sensitive to tunneling, frequency changes along the reaction path, and variational effects, and

thus can be another critical test of the accuracy of the MCMM method, although, as a caution, we note that heavy-atom isotope effects require very high precision, and the present method has been tested most thoroughly as far as its usefulness for problems requiring a precision level of 10−20%, which is typical experimental accuracy for absolute rate constants (in favorable cases). Furthermore, one expects that primary KIEs will be easier than secondary KIEs. Finally, we note that MCMM is a very general method, and its applications are not limited to the VTST examples studied in this article; other studies, e.g., trajectory calculations based on MCMM potential energy surfaces, will also be good directions to pursue. These will be interesting topics to explore in the future.

**Acknowledgment.** This work was supported in part by the U.S. Department of Energy, Office of Basic Energy Sciences. H.L. thanks the Minnesota Supercomputing Institute for a Research Scholarship.

**Supporting Information Available:** Tables reviewing the sequence for adding supplementary points in the standard MCMM scheme(Table S-1),[51] the direct dynamics and MCMM-10 rate constants for all six reactions at additional temperatures (Tables S-2−S-7) (in addition to 300, 400, and 500 K, which are given in Tables 3−8), along with the results for decreasing FC to 5 $cm^{-1}$ for reaction R-6 (Table S-8), the locations of supplementary Shepard points in all the MCMM dynamics calculations (Table S-9), the percentage deviation of the MCMM reaction rates as compared with direct dynamics calculations at six temperatures for each reaction (Table S-10), and the bottleneck properties at 200 K (in addition to at 300 K, which are given in Table 10) for the hydrogen-transfer reaction of OH with $CH_4$ by direct dynamics and MCMM-10/10a (Table S-11). This material is available free of charge via the Internet at http://pubs.acs.org.

## References and Notes

(1) Garrett, B. C.; Truhlar, D. G.; Grev, R. S.; Magnuson, A. W. *J. Phys. Chem.* **1980**, *84*, 1730.
(2) Garrett, B. C.; Truhlar, D. G. *J. Chem. Phys.* **1984**, *81*, 309.
(3) Truhlar, D. G.; Garrett, B. C.; Hipes, P. G.; Kuppermann, A. *J. Chem. Phys.* **1984**, *81*, 3542.
(4) Truhlar, D. G.; Isaacson, A. D.; Garrett, B. C. In *Theory of Chemical Reaction Dynamics*; Baer, M., Ed.; CRC Press: Boca Raton, FL, 1985; Vol. 4; p 65.
(5) Kreevoy, M. M.; Truhlar, D. G. In *Investigation of Rates and Mechanisms of Reactions*; Bernasconi, C. F., Ed.; John Wiley & Sons: New York, 1986; Vol. 6; p 13.
(6) Tucker, S. C.; Truhlar, D. G. In *New Theoretical Concepts Understanding Organic Reactions*; Csizmadia, I. G., Bertran, J., Eds.; NATO ASI Series, Vol. 267. Kluwer Academic Publishers: Dordrecht, The Netherlands, 1989; p 291.
(7) Truhlar, D. G.; Garrett, B. C.; Klippenstein, S. J. *J. Phys. Chem.* **1996**, *100*, 12771.
(8) Allison, T. C.; Truhlar, D. G. In *Modern Methods for Multidimensional Dynamics Computations in Chemistry*; Thompson, D. L., Ed.; World Scientific: Singapore, 1998; p 618.
(9) Truhlar, D. G.; Gordon, M. S. *Science* **1990**, *249*, 491.
(10) Pople, J. A.; Binkley, J. S.; Seeger, R. *Int. J. Quantum Chem., Symp.* **1976**, *10*, 1.
(11) Purvis, G. D., III; Bartlett, R. J. *J. Chem. Phys.* **1982**, *76*, 1910.
(12) Raghavachari, K.; Trucks, G. W.; Pople, J. A.; Head-Gordon, M. *Chem. Phys. Lett.* **1989**, *157*, 479.
(13) Hirao, K. *Chem. Phys. Lett.* **1992**, *190*, 374.
(14) Raghavachari, K.; Anderson, J. B. *J. Phys. Chem.* **1996**, *100*, 12960.
(15) *Chemical Applications of Density-Functional Theory*; Laird, B. B., Ross, R. B., Ziegler, T., Eds.; ACS Symposium Series 629. American Chemical Society: Washington, DC, 1996.
(16) Curtiss, L. A.; Raghavachari, K.; Redfern, P. C.; Rassolov, V.; Pople, J. A. *J. Chem. Phys.* **1998**, *109*, 7764.
(17) Curtiss, L. A.; Raghavachari, K.; Redfern, P. C.; Pople, J. A. *J. Chem. Phys.* **2000**, *112*, 1125.
(18) Fast, P. L.; Sanchez, M. L.; Truhlar, D. G. *Chem. Phys. Lett.* **1999**, *306*, 407.
(19) Fast, P. L.; Corchado, J. C.; Sanchez, M. L.; Truhlar, D. G. *J. Phys. Chem. A* **1999**, *103*, 5129.
(20) Lynch, B. J.; Fast, P. L.; Harris, M.; Truhlar, D. G. *J. Phys. Chem. A* **2000**, *104*, 4811.
(21) Brooks, B. R.; Bruccoleri, R. E.; Olafson, B. D.; States, D. J.; Swaminathan, S.; Karplus, M. *J. Comput. Chem.* **1983**, *4*, 187.
(22) Allinger, N. L.; Yuh, Y. H.; Lii, J. H. *J. Am. Chem. Soc.* **1989**, *111*, 8551.
(23) Lii, J. H.; Allinger, N. L. *J. Am. Chem. Soc.* **1989**, *111*, 8566.
(24) Lii, J. H.; Allinger, N. L. *J. Am. Chem. Soc.* **1989**, *111*, 8576.
(25) Pearlman, D. A.; Case, D. A.; Caldwell, J. W.; Ross, W. S.; Cheatham, T. E., III; DeBolt, S.; Ferguson, D.; Seibel, G.; Kollman, P. *Comput. Phys. Commun.* **1995**, *91*, 1.
(26) Halgren, T. A. *J. Comput. Chem.* **1996**, *17*, 490.
(27) Warshel, A.; Karplus, M. *Chem. Phys. Lett.* **1975**, *32*, 11.
(28) Leforestier, C. *J. Chem. Phys.* **1978**, *68*, 4406.
(29) Truhlar, D. G.; Duff, J. W.; Blais, N. C.; Tully, J. C.; Garrett, B. C. *J. Chem. Phys.* **1982**, *77*, 764.
(30) Car, R.; Parrinello, M. *Phys. Rev. Lett.* **1985**, *55*, 2471.
(31) Baldridge, K. K.; Gordon, M. S.; Steckler, R.; Truhlar, D. G. *J. Phys. Chem.* **1989**, *93*, 5107.
(32) Galli, G.; Parrinello, M. *NATO ASI Ser., Ser. E* **1991**, *205*, 283.
(33) Gonzalez-Lafont, A.; Truong, T. N.; Truhlar, D. G. *J. Phys. Chem.* **1991**, *95*, 4618.
(34) Hartke, B.; Carter, E. A. *J. Chem. Phys.* **1992**, *97*, 6569.
(35) Liu, Y. P.; Lynch, G. C.; Truong, T. N.; Lu, D. H.; Truhlar, D. G.; Garrett, B. C. *J. Am. Chem. Soc.* **1993**, *115*, 2408.
(36) Liu, Y. P.; Lu, D. H.; Gonzalez-Lafont, A.; Truhlar, D. G.; Garrett, B. C. *J. Am. Chem. Soc.* **1993**, *115*, 7806.
(37) Truong, T. N.; Lu, D.-h.; Lynch, G. C.; Liu, Y.-P.; Melissas, V. S.; Stewart, J. J. P.; Steckler, R.; Garrett, B. C.; Isaacson, A. D.; Gonzalez-Lafont, A.; Rai, S. N.; Hancock, G. C.; Joseph, T.; Truhlar, D. G. *Comput. Phys. Commun.* **1993**, *75*, 143.
(38) Truhlar, D. G. In *The Reaction Path in Chemistry: Current Approaches and Perspectives*; Heidrich, D., Ed.; Kluwer: Dordrecht, The Netherlands, 1995; Vol. 16; p 229.
(39) Cheng, H. P.; Barnett, R. N.; Landman, U. *Chem. Phys. Lett.* **1995**, *237*, 161.
(40) Truong, T. N. *J. Chem. Phys.* **1995**, *102*, 5335.
(41) Gordon, M. S.; Chaban, G.; Taketsugu, T. *J. Phys. Chem.* **1996**, *100*, 11512.
(42) Bueker, H.-H.; Helgaker, T.; Ruud, K.; Uggerud, E. *J. Phys. Chem.* **1996**, *100*, 15388.
(43) Cheng, H.-P.; Krause, J. L. *J. Chem. Phys.* **1997**, *107*, 8461.
(44) Aida, M.; Yamataka, H.; Dupuis, M. *Chem. Phys. Lett.* **1998**, *292*, 474.
(45) Duncan, W. T.; Bell, R. L.; Truong, T. N. *J. Comput. Chem.* **1998**, *19*, 1039.
(46) Roberto-Neto, O.; Coitino, E. L.; Truhlar, D. G. *J. Phys. Chem. A* **1998**, *102*, 4568.
(47) Corchado, J. C.; Espinosa-Garcia, J.; Roberto-Neto, O.; Chuang, Y.-Y.; Truhlar, D. G. *J. Phys. Chem. A* **1998**, *102*, 4899.
(48) Bolton, K.; Schlegel, H. B.; Hase, W. L.; Song, K. *Phys. Chem. Chem. Phys.* **1999**, *1*, 999.
(49) Truong, T. N.; Maity, D. K. *Comput. Chem. (Singapore, Singapore)* **2000**, *5*, 211.
(50) Kim, Y.; Corchado, J. C.; Villa, J.; Xing, J.; Truhlar, D. G. *J. Chem. Phys.* **2000**, *112*, 2718.
(51) Albu, T. V.; Corchado, J. C.; Truhlar, D. G. *J. Phys. Chem.* **2001**, *105*, 8465.
(52) London, F. *Z. Electrochem.* **1929**, *35*, 552.
(53) Eyring, H.; Polanyi, M. *Z. Phys. Chem.* **1931**, *B12*, 279.
(54) Sato, S. *Bull. Chem. Soc. Jpn.* **1955**, *28*, 450.
(55) Yasunori, I. *Bull. Chem. Soc. Jpn.* **1959**, *32*, 1110.
(56) Ellison, F. O. *J. Am. Chem. Soc.* **1963**, *85*, 3540.
(57) Parr, C. A.; Truhlar, D. G. *J. Phys. Chem.* **1971**, *75*, 1844.
(58) Blais, N. C.; Truhlar, D. G. *J. Chem. Phys.* **1973**, *58*, 1090.
(59) Raff, L. M. *J. Chem. Phys.* **1974**, *60*, 2220.
(60) Tully, J. C. In *Semiempirical Methods of Electronic Structure Theory, Part A: Techniques*; Segal, G. A., Ed.; Plenum: New York, 1977; p 173.
(61) Truhlar, D. G.; Wyatt, R. E. *Adv. Chem. Phys.* **1977**, *36*, 141.
(62) Kuntz, P. J. In *Atom-Molecule Collision Theory*; Bernstein, R. B., Ed.; Plenum: New York, 1979; p 79.
(63) Faist, M. B.; Muckerman, J. T. *J. Chem. Phys.* **1979**, *71*, 225.
(64) Vila, C. L.; Kinsey, J. L.; Ross, J.; Schatz, G. C. *J. Chem. Phys.* **1979**, *70*, 2414.
(65) Warshel, A.; Weiss, R. M. *J. Am. Chem. Soc.* **1980**, *102*, 6218.
(66) Zeiri, Y.; Shapiro, M. *J. Chem. Phys.* **1981**, *75*, 1170.
(67) Pross, A.; Shaik, S. S. *Acc. Chem. Res.* **1983**, *16*, 363.

(68) Duggan, J. J.; Grice, R. *J. Chem. Soc., Faraday Trans. 2* **1984**, *80*, 739.

(69) Garrett, B. C.; Truhlar, D. G. *J. Chem. Phys.* **1985**, *82*, 4543.

(70) Sevin, A. *NATO ASI Ser., Ser. C* **1986**, *176*, 235.

(71) Bernardi, F.; McDouall, J. J. W.; Robb, M. A. *J. Comput. Chem.* **1987**, *8*, 296.

(72) Bernardi, F.; Olivucci, M.; McDouall, J. J. W.; Robb, M. A. *J. Am. Chem. Soc.* **1987**, *109*, 544.

(73) Warshel, A.; Sussman, F.; Hwang, J. K. *J. Mol. Biol.* **1988**, *201*, 139.

(74) Chang, Y. T.; Miller, W. H. *J. Phys. Chem.* **1990**, *94*, 5884.

(75) Warshel, A. *Computer Modeling of Chemical Reactions in Enzymes and Solutions*; John Wiley & Sons: New York, 1991.

(76) Yadav, A.; Jackson, R. M.; Holbrook, J. J.; Warshel, A. *J. Am. Chem. Soc.* **1991**, *113*, 4800.

(77) Kabbaj, O. K.; Lepetit, M. B.; Malrieu, J. P.; Sini, G.; Hiberty, P. C. *J. Am. Chem. Soc.* **1991**, *113*, 5619.

(78) Cimiraglia, R. *NATO ASI Ser., Ser. B* **1992**, *299*, 11.

(79) Chang, Y. T.; Minichino, C.; Miller, W. H. *J. Chem. Phys.* **1992**, *96*, 4341.

(80) Benneyworth, P. R.; Balint-Kurti, G. G.; Davis, M. J.; Williams, I. H. *J. Phys. Chem.* **1992**, *96*, 4346.

(81) Åqvist, J.; Warshel, A. *Chem. Rev.* **1993**, *93*, 2523.

(82) Shaik, S.; Reddy, A. C. *J. Chem. Soc., Faraday Trans.* **1994**, *90*, 1631.

(83) Mathis, J. R.; Bianco, R.; Hynes, J. T. *J. Mol. Liq.* **1994**, *61*, 81.

(84) Kong, Y. S.; Warshel, A. *J. Am. Chem. Soc.* **1995**, *117*, 6234.

(85) Mestres, J.; Hiberty, P. C. *New J. Chem.* **1996**, *20*, 1213.

(86) Åqvist, J. In *Computational Approaches to Biochemical Reactivity*; Naray-Szabo, G.; Warshel, A., Eds.; Kluwer Academic: Dordrecht, The Netherlands, 1997; Vol. 19; p 341.

(87) Allison, T. C.; Mielke, S. L.; Schwenke, D. W.; Truhlar, D. G. *J. Chem. Soc., Faraday Trans.* **1997**, *93*, 825.

(88) Minichino, C.; Voth, G. A. *J. Phys. Chem. B* **1997**, *101*, 4544.

(89) Cattaneo, P.; Persico, M. *Chem. Phys.* **1997**, *214*, 49.

(90) Bottoni, A. *J. Phys. Chem. A* **1998**, *102*, 10142.

(91) Dobrovsky, I.; Levine, R. D. *Chem. Phys. Lett.* **1998**, *286*, 155.

(92) Kolmodin, K.; Hansson, T.; Danielsson, J.; Aqvist, J. *ACS Symp. Ser.* **1999**, *721*, 370.

(93) Anglada, J. M.; Besalu, E.; Bofill, J. M.; Crehuet, R. *J. Comput. Chem.* **1999**, *20*, 1112.

(94) Mo, Y.; Gao, J. *J. Phys. Chem. A* **2000**, *104*, 3012.

(95) Nakamura, H.; Truhlar, D. G. *J. Chem. Phys.* **2001**, *115*, 10353.

(96) Truhlar, D. G. *J. Phys. Chem. A* **2002**, *106*, 5048.

(97) Lu, D.-h.; Truong, T. N.; Melissas, V. S.; Lynch, G. C.; Liu, Y.-P.; Garrett, B. C.; Steckler, R.; Isaacson, A. D.; Rai, S. N.; Hancock, G. C.; Lauderdale, J. G.; Joseph, T.; Truhlar, D. G. *Comput. Phys. Commun.* **1992**, *71*, 235.

(98) Garrett, B. C.; Truhlar, D. G.; Wagner, A. F.; Dunning, T. H., Jr. *J. Chem. Phys.* **1983**, *78*, 4400.

(99) Bondi, D. K.; Connor, J. N. L.; Garrett, B. C.; Truhlar, D. G. *J. Chem. Phys.* **1983**, *78*, 5981.

(100) Garrett, B. C.; Abusalbi, N.; Kouri, D. J.; Truhlar, D. G. *J. Chem. Phys.* **1985**, *83*, 2252.

(101) Kreevoy, M. M.; Ostovic, D.; Truhlar, D. G.; Garrett, B. C. *J. Phys. Chem.* **1986**, *90*, 3766.

(102) Garrett, B. C.; Joseph, T.; Truong, T. N.; Truhlar, D. G. *Chem. Phys.* **1989**, *136*, 271.

(103) Fernandez-Ramos, A.; Truhlar, D. G. *J. Chem. Phys.* **2001**, *114*, 1491.

(104) Ischtwan, J.; Collins, M. A. *J. Chem. Phys.* **1994**, *100*, 8080.

(105) Nguyen, K. A.; Rossi, I.; Truhlar, D. G. *J. Chem. Phys.* **1995**, *103*, 5522.

(106) Garrett, B. C.; Truhlar, D. G. *J. Am. Chem. Soc.* **1979**, *101*, 4534.

(107) March, J. *Advanced Organic Chemistry: Reactions, Mechanisms, and Structure*, 4th ed.; John Wiley & Sons: New York, 1992.

(108) Frisch, M. J.; Trucks, G. W.; Schlegel, H. B.; Scuseria, G. E.; Robb, M. A.; Cheeseman, J. R.; Zakrzewski, V. G.; Montgomery, J. A., Jr.; Stratmann, R. E.; Burant, J. C.; Dapprich, S.; Millam, J. M.; Daniels, A. D.; Kudin, K. N.; Strain, M. C.; Farkas, O.; Tomasi, J.; Barone, V.; Cossi, M.; Cammi, R.; Mennucci, B.; Pomelli, C.; Adamo, C.; Clifford, S.; Ochterski, J.; Petersson, G. A.; Ayala, P. Y.; Cui, Q.; Morokuma, K.; Salvador, P.; Dannenberg, J. J.; Malick, D. K.; Rabuck, A. D.; Raghavachari, K.; Foresman, J. B.; Cioslowski, J.; Ortiz, J. V.; Baboul, A. G.; Stefanov, B. B.; Liu, G.; Liashenko, A.; Piskorz, P.; Komaromi, I.; Gomperts, R.; Martin, R. L.; Fox, D. J.; Keith, T.; Al-Laham, M. A.; Peng, C. Y.; Nanayakkara, A.; Gonzalez, C.; Challacombe, M.; Gill, P. M. W.; Johnson, B. G.; Chen, W.; Wong, M. W.; Andres, J. L.; Head-Gordon, M.; Replogle, E. S.; Pople, J. A. Gaussian98 (Revision A.11); Gaussian, Inc.: Pittsburgh, PA, 2001.

(109) Lynch, B. J.; Zhao, Y.; Truhlar, D. G. *J. Phys. Chem. A* **2003**, *107*, 1384.

(110) Although we include the reactant spin−orbit splitting in the reactant electronic partition function, we neglect its effect (about 0.2 kcal/mol) on the barrier height and energy of reaction for reaction reactions R-1, R-2, R-5, and R-6.

(111) Jackels, C. F.; Gu, Z.; Truhlar, D. G. *J. Chem. Phys.* **1995**, *102*, 3188.

(112) Nguyen, K. A.; Jackels, C. F.; Truhlar, D. G. *J. Chem. Phys.* **1996**, *104*, 6491.

(113) Chuang, Y.-Y.; Truhlar, D. G. *J. Phys. Chem. A* **1998**, *102*, 242.

(114) Corchado, J. C.; Chuang, Y.-Y.; Coitiño, E. L.; Truhlar, D. G. gaussrate 9.0, University of Minnesota, Minneapolis, MN, 2002.

(115) Corchado, J. C.; Chuang, Y.-Y.; Fast, P. L.; Villà, J.; Hu, W.-P.; Liu, Y.-P.; Lynch, G. C.; Nguyen, K. A.; Jackels, C. F.; Melissas, V. S.; Lynch, B. J.; Rossi, I.; Coitiño, E. L.; Fernandez-Ramos, A.; Pu, J.; Albu, T. V.; Steckler, R.; Garrett, B. C.; Isaacson, A. D.; Truhlar, D. G. polyrate 9.1, University of Minnesota, Minneapolis, MN, 2002.

(116) Page, M.; McIver, J. W., Jr. *J. Chem. Phys.* **1988**, *88*, 922.

(117) Albu, T. V.; Corchado, J. C.; Kim, Y.; Villà, J.; Xing, J.; Lin, H.; Truhlar, D. G. mc-tinkerate 9.1, University of Minnesota, Minneapolis, MN, 2003.

(118) Corchado, J. C.; Kim, Y.; Villà, J.; Albu, T. V.; Xing, J.; Truhlar, D. G. tinkerate 8.5, University of Minnesota, Minneapolis, MN, 2000.

(119) Albu, T. V.; Corchado, J. C.; Kim, Y.; Villà, J.; Xing, J.; Lin, H.; Truhlar, D. G. mc-tinker 1.0.1, University of Minnesota, Minneapolis, MN, 2003.

(120) Ponder, J. W. tinker 3.5, Washington University, St. Louis, MO, 1997.

(121) Along the MEP for reaction R-2, a step size of 0.002 $a_0$ for the gradient and 0.02 $a_0$ for the Hessian were used for calculating the rates in MCMM-$N_s$ ($N_s$ = 8, 9, and 10) in order to avoid an unphysical oscillation of the generalized normal-mode frequencies around $s = -0.19$ $a_0$. The occasional occurrence of such oscillations has been discussed in ref 50.

(122) CVT is very sensitive to any structure in the free energy profile, but one can expect that this sensitivity will essentially always be reduced by a tunneling calculation. The reason is that, in general, calculations (like tunneling) that involve integrals are likely to be more stable and robust than methods that involving the maximum of a curve, since integration averages out fluctuations.

(123) The optimization for the saddle point, which is always needed for all dynamics methods (direct dynamics, standard MCMM dynamics, and the improved MCMM dynamics using partial Hessians) and even for a reliable calculation of the barrier height, is a separate issue, and its cost is not considered here. However, we did take into account the cost of the saddle point normal mode calculation, which is dominated by the cost of the Hessian.

(124) Ishida, T.; Schatz, G. C. *Chem. Phys. Lett.* **1999**, *314*, 369.

(125) Gao, J. *Acc. Chem. Res.* **1996**, *29*, 298.

(126) Merz, K. M. Jr. In *Combined Quantum Mechanical and Molecular Mechanical Methods*; Gao, J., Thompson, M. A., Eds.; ACS Symposium Series 712, American Chemical Society: Washington, DC, 1998; p 2.

(127) Antes, I.; Thiel, W. In *Combined Quantum Mechanical and Molecular Mechanical Methods*; Gao, J., Thompson, M. A., Eds.; ACS Symposium Series 712, American Chemical Society: Washington, DC, 1998; p 50.

(128) Gao, J.; Truhlar, D. G. *Annu. Rev. Phys. Chem.* **2002**, *53*, 467.

(129) Pu, J.; Truhlar, D. G.; Gao, J. *J. Phys. Chem. A* **2004**, *108*, 632.

(130) Maseras, F.; Morokuma, K. *J. Comput. Chem.* **1995**, *16* 1170.

(131) Matsubara, T.; Maseras, F.; Koga, N.; Morokuma, K. *J. Phys. Chem.* **1996**, *100*, 2573.

(132) Humbel, S.; Sieber, S.; Morokuma, K. *J. Chem. Phys.* **1996**, *105*, 1959.

(133) Coitiño, E. L.; Truhlar, D. G.; Morokuma, K. *Chem. Phys. Lett.* **1996**, *259*, 159.

(134) Corchado, J. C.; Truhlar, D. G. In ref 126, p 106.

(135) Cui, Q.; Guo, H.; Karplus, M. *J. Chem. Phys.* **2002**, *117*, 5617.

(136) Lauderdale, J. G.; Truhlar, D. G. *J. Chem. Phys.* **1986**, *84*, 192.

(137) Garcia-Viloca, M.; Alhambra, C.; Truhlar, D. G.; Gao, J. *J. Chem. Phys.* **2001**, *114*, 9953.

(138) Alhambra, C.; Corchado, J.; Sánchez, M. L.; Garcia-Viloca, M.; Gao, J.; Truhlar, D. G. *J. Phys. Chem. B* **2001**, *105*, 11326.

(139) Liu, H.; Jensen, J. H. *Theor. Chem. Acc.* **2002**, *107*, 211.

(140) Jin, S.; Head, J. D. *Surf. Sci.* **1994**, *318*, 204.

(141) Calvin, M. D.; Head, J. D.; Jin, S. *Surf. Sci.* **1996**, *345*, 161.